Testing and Optimization of an Automated Air Sampling System for the Future Air Sampling Network of the Integrated Carbon Observation System (ICOS)

DIPLOMA THESIS

by

Stephan Baum

Mat.Nr.: 481158

born 18 December 1980

Supervised by

Dr. habil. Christoph Gerbig

Prof. Dr. rer. nat. Bernd Rudolph

Submitted on 29 June 2010

Presented as a part of the requirements

to gain the academic degree

GRADUATE ENGINEER

at the

Department of SciTec - Precision - Optics - Material - Environment

University of Applied Sciences Jena, Germany

“Learning and innovation go hand in hand. The arrogance of success is to think that what you did yesterday will be sufficient for tomorrow.“

- William G. Pollard (1911-1989), American Physicist -

Abstract

The Department for Biogeochemical Systems of the Max-Planck-Institute for Biogeochemistry in Jena is a key player in the development and construction of the research infrastructure of the Integrated Carbon Observation System (ICOS) in Europe. Among others, the institute is responsible for the evaluation of a commercially available air sampling system that makes it possible to automize the sampling process. It is planned to use the system in an unattended, and low-maintenance scenario within a network of terrestrial atmospheric monitoring stations. Such a sampling approach promises a greater capacity to deepen the scientific knowledge on carbon cycle processes.

Since the instrument was originally designed for aircraft installation, it is necessary to assess if the system is suitable to serve as a reliable flask sampler at a fixed, ground-based platform. This diploma thesis describes the automated flask sampling system and associated tests, followed by a discussion about necessary steps that need to be taken to successfully integrate the system into the ICOS Atmospheric Station.

A technical approach is presented to retrofit the sampling containers with commercially available flask seals. This will reduce the influence of permeation and will maintain the sample integrity if flasks are exposed to long storage periods. In addition, several laboratory tests have been conducted to better assess the system performance of the sampler. One experiment was concerned with the investigation of memory effects possibly induced by the corrugated tubing inside the instrument. The results indicated that there is no discernible memory effect for several atmospheric gas species which will also be covered in the frame of the

future ICOS flask sampling program. A second experiment was performed to assess the quality of flask samples derived from the automated air sampling system to validate continuous measurements from a cavity ring-down analyzer. The results have revealed a high correlation between flask and continuous data. Nevertheless, in its basic configuration the automated air sampling system is only capable to capture atmospheric events within few seconds. The main cause for this is the high sample flow rate created by the two-stage compressor, which is dimensioned for aircraft-borne platforms. This restricts the comparability between flask data and continuous measurements which are carried out by using the integrating effect of air buffer volumes. Therefore, it will be necessary to reduce the sample flow rate since it is envisioned to include the aforementioned method into the design of the ICOS Atmospheric Station.

The work on this instrument is not yet completed. Comprehensive test with the integrated air drying unit have to be carried out and several improvements are required for operating the automated air sampling system in a stationary, unattended, and low-maintenance scenario within the ICOS infrastructure.

Table of Contents

Chapter 1

Introduction

1.1 Automated Flask Sampling: A Necessary Step in Enhancing Monitoring Strategies in Global Carbon Cycle Research

The periodic collection of whole air in glass flasks for subsequent laboratory analysis has proven to be a tool of major importance in global carbon cycle research. Over the last decades, a large reliable data set of long-term flask records has come into existence providing important information about the seasonal and interannual variability of atmospheric CO_2 and other greenhouse gases (GHGs) as well as their spatial distribution [e.g. 1-3]. To date, the number of terrestrial flask sampling sites over the world has increased substantially, and flask sampling campaigns on moving platforms (e.g. ships, aircraft) have been intensified [e.g. 4]. Furthermore, numerous academic institutions have connected their established flask sampling stations into a global network of sites. The most prominent example is the Cooperative Air Sampling Network of the National Oceanic and Atmospheric Administration/Earth System Research Laboratory (NOAA/ESRL), being the largest existing network of this type.

Flask sampling offers several operational and scientific advantages over continuous measurement systems, and it is the preferred observational method for remote areas where it can be difficult to comply all necessary requirements for in-

situ measurements (e.g electrical power supply, keeping and maintaining of a gas handling system for regular instrument calibration). In general, it is less costly to maintain and calibrate only a single set of instruments in a central laboratory for flask analysis than a large number of continuous analyzers in a network of specific sampling location. Furthermore, discrete sampling is often the first step to identify high-quality background sites for upgrading them to continuous monitoring stations, and the storage of flasks makes it even possible to analyze them after new measurement techniques are developed and become available [5].

Owing to advancements in analytical instrumentation less sample air is nowadays needed. These improvements allow for analyzing a single flask sample for several climate-relevant species [6]. In addition to this, whole air samples provide important information about the isotopic signatures of CO_2 and CH_4. Furthermore, measurements of stable isotopic ratios can only be carried out with mass spectrometers which are currently not suitable for field deployment because they are too expensive and complex to operate and require too much time and effort on the maintenance level. Therefore, flask sampling is an indispensable tool to identify sources and sinks and to quantify ecosystem-atmosphere interactions of climatically important species [e.g. 7, 8].

The simplest way to obtain a flask sample is to evacuate the sampling container in the laboratory and get it filled by just opening the stopcock at the sampling location, a method that is still successfully in use in one of the global networks for atmospheric oxygen measurements [9]. Alternatively, it has become established practice to collect air samples in preconditioned flasks in a pass-through displacement mode by means of an active air sampling system. The essential parts of such an active air sampling system are a battery-powered pumping unit to provide a constant flow of sample air, a back pressure regulator and valve arrangement for flask pressurizing, and a drying cartridge, usually filled with

anhydrous magnesium perchlorate, to dry the air prior to filling [10]. However, both described methods of collecting whole air samples are manual techniques, and thus constrained by the need of personnel who has to be present on the spot to follow the sampling protocol. In practice, this involves considerable time and effort on the part of the operator, which limits sampling frequency and duration to seasonal observation capacities. Furthermore, important requirements on the moment of sampling, such as well mixed-atmospheric conditions or a minimum of wind speed from a preferred wind direction, cannot always be met by the sampling operator.

The one practical solution to circumvent the above mentioned problems might be the use of automated flask sampling systems. Automated flask samplers allow for the samples to be collected without having personnel attention and can afford a much greater temporal frequency of sampling, which is a prerequisite for event-based sampling as well as for nighttime measurements for Keeling plot applications [e.g. 11, 12]. Furthermore, the sampling frequency can be tailored to the individual attributes of the sampling location (e.g. latitude, altitude, influence of possible point sources, ground-based or moving platform). In this respect, the required sampling schedule at terrestrial sites has to be more frequent than at oceanic sites since CO_2 mixing ratios are much less variable in marine areas than over terrestrial surfaces where carbon-fluxes tend to be more dynamic [13, 14]. By using automated flask samplers, the sampling interval can be extended to be more representative for the mean daily flux of CO_2 at a certain sampling plot. On the other hand, automatic air samplers are more expensive and require higher maintenance than manual sampling systems. Additionally, a minimum of infrastructure on the sampling site is needed since unattended sampling can potentially occur over weeks.

Over recent years, several efforts have been made in the development of automated air sampling systems. A typical example is the continuous air drying and flask sampling system of the Centre for Isotope Research, Groningen, Netherlands which operates at various ground-based sampling sites in Europe and is capable to run without servicing for periods of more than one month [11, 15]. Nevertheless, most efforts with similar purposes were directed towards the automated collection of whole air samples aboard aircraft and in the frame of ecosystem-scale measurements [e.g. 4, 13]. Presently, the use of such instruments on ground-based monitoring platforms in most of the global air sampling networks is still marginal.

Today it is widely accepted that there is a close relationship between global warming and growing anthropogenic emissions of CO_2 and other gases that absorb infrared radiation [16]. Rising temperatures, changing precipitation patterns, sea level rise and ocean acidification are just a few manifestations of climate change caused by human activities. In this context, global monitoring networks have a growing relevance to policy decision making since the collected data is of crucial importance to quantify anthropogenic emissions of greenhouse gases and to report trends in global climate change. Consequently, there is a strong need to expand existing air sampling networks and to establish more sophisticated monitoring systems [17]. However, this is associated with a significant increase in the number of flask samples that need to be processed and - without any remarkable increase in manpower - this can only be achieved by further automation of atmospheric air sampling technologies.

1.2 Goals of the Thesis

This work was performed as part of the preparatory phase of the Integrated Carbon Observation System project funded under the EU Framework VII Programme Grant Agreement No. 211574. During the ICOS preparatory phase a subset of instruments will be tested and evaluated with the objective to install them into a network of ground-based platforms for atmospheric monitoring. One integral part of the atmospheric measurement strategy is the use of an automated flask sampling system which was originally designed to collect whole air samples aboard small aircraft. In order to use such an instrument as a reliable tool for atmospheric trace gas sampling at a fixed site a detailed assessment of the quality and functionality of the system is necessary. This includes careful laboratory testing as well as optimization of the instrument to improve its effectiveness when used on a routine basis. In this regard, the main goals of this thesis were:

- Development of a technical approach to improve the storage characteristics of the sampling containers which are installed in the air sampling system.
- Investigation of instrumental factors that might have the potential to affect the integrity of the sampling process.
- Assessment of the suitability to validate in-situ measurements through flask samples obtained from the instrument.
- Elaboration of strategies for further enhancements of the instrument to better meet the requirements for the stationary ground-based installation at an atmospheric observatory.

Chapter 2

Background

2.1 The ICOS Research Project

This section is giving a brief description of the basic strategy and the main objectives of the Integrated Carbon Observation System (ICOS). For more detailed information, the interested reader is recommended to visit the official ICOS webpage (http://www.icos-infrastructure.eu).

2.1.1 Basic Characterization of the ICOS Research Project

ICOS is an ESFRI (European Strategy Forum of Research Infrastructures) infrastructure project under the Seventh Framework Programme of the European Commission. The project aims to build up a standardized, high-precision long-term network of observatories for quantifying and understanding the greenhouse gas balance over the European continent and neighbouring regions. For that, ICOS will combine different observational strategies in the terrestrial, marine and atmospheric compartments. The ICOS infrastructure initiative is based on research tools, techniques and design studies which have been developed and pioneered

during former European research projects. Referring to this, ICOS wants to join forces, for instance with CarboEurope-IP, which has ended in November 2008, and the ongoing IMECC (Infrastructure for Measurements of the European Carbon Cycle) project.

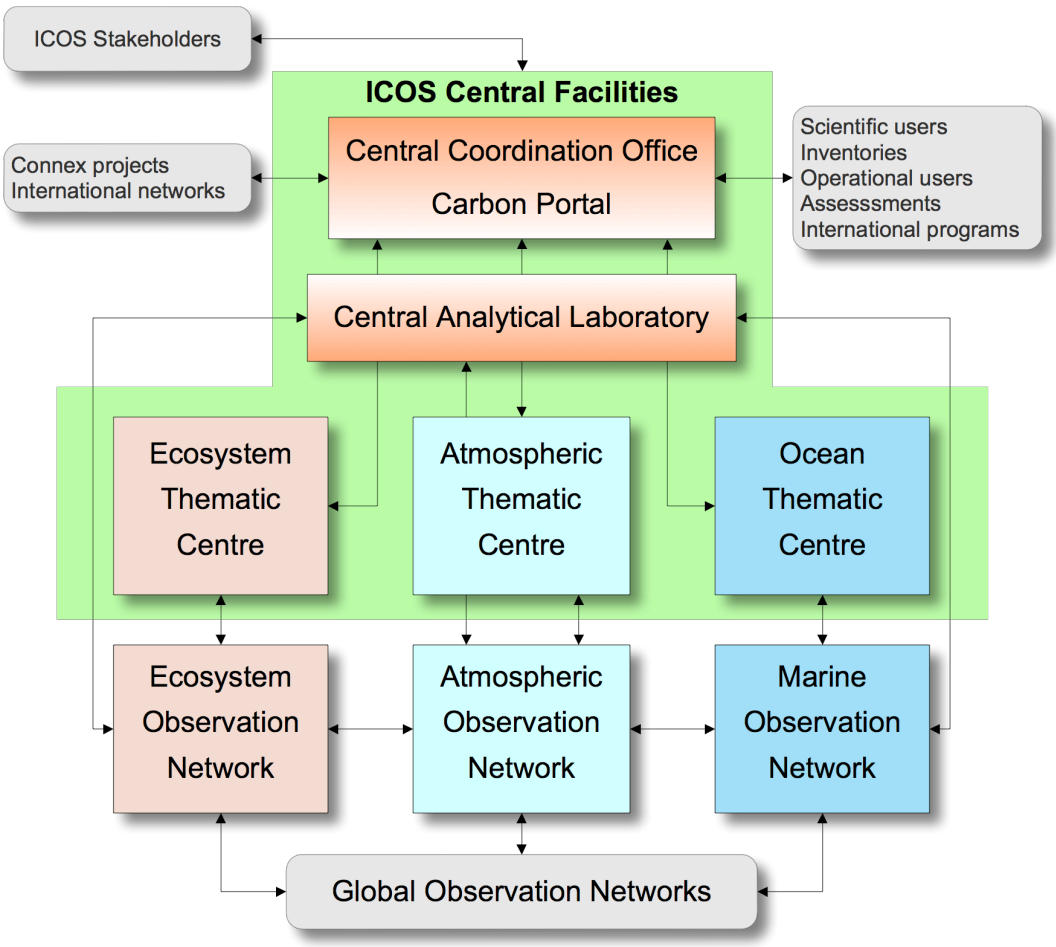

Figure 1 Organization of the ICOS infrastructure. (Redrawn from [18])

Different central facilities will be responsible to organize the numerous scientific activities within the ICOS infrastructure. A Central Coordination Office will ensure the management of the infrastructure and will be responsible for the establishment of a data acquisition center (Carbon Portal) to provide free access to the collected ICOS data (see Fig. 1).

As illustrated in Figure 1, another key element of ICOS will be the Central Analytical Laboratory (CAL). The CAL will be developed under the guidance of the Max-Planck-Institute for Biogeochemistry (MPI-BGC) in Jena and the Institute for Environmental Physics at the Universtiy of Heildelberg, and it is planned to locate it in Germany. The facility will consist of three laboratories, which are the Central Calibration and Standards Laboratory and the Laboratories for Radiocarbon and Flask Analysis. Main services of the CAL will be the preparation of working gas standards (~200 per year [18]) to calibrate the atmospheric measurement systems at the in-situ observatories, the conditioning and distribution of flasks as well as their analysis for different climate-relevant gas species (see Sec. 2.2). The total number of discrete air samples that will be obtained from atmospheric stations and through regular aircraft sampling is estimated to be around 8000 flasks per year [18]. All three laboratories will participate in international intercomparison exercises, in order to meet the requirements according to the guidelines of the Global Atmosphere Watch Quality Assurance System of the World Meteorological Organisation.

The ICOS monitoring network will be a distribution of numerous measurement sites across Europe. Three sub-networks, the Atmospheric Concentration Network, the Ecosystem Flux Network and the Network of Marine Observations, will form the infrastructural basis in order to provide high-precision measurements of ecosystem fluxes and atmospheric concentration of CO_2 and other GHGs, combined with additional measurement parameters. Each monitoring station will be equipped with a standardised set of instruments to ensure that measurements are collected in a consistent way. This will allow for generating highly reproducible results and guaranteeing the comparability of the collected data among the stations.

The ICOS Atmospheric Concentration Network will comprise about 30 primary sites chosen for installing an atmospheric observatory that will be representative of a footprint area of more than 100 km^2 [19]. Each station will consist of commercially available instruments for the determination of greenhouse gas concentrations, planetary boundary layer height and meteorological parameters (e.g. wind speed and direction, relative humidity, temperature, atmospheric pressure). Furthermore, the continuos in-situ GHG measurements will be complemented with a periodic flask sampling program by means of an automatic flask sampling system. Figure 2 shows the basic design concept of the ICOS Atmospheric Station (ICOS AS). The main features of the ICOS AS will be: standardization of equipment and methods, automatic operation, reduced calibration and maintenance effort, local and remote control, as well as modularity.

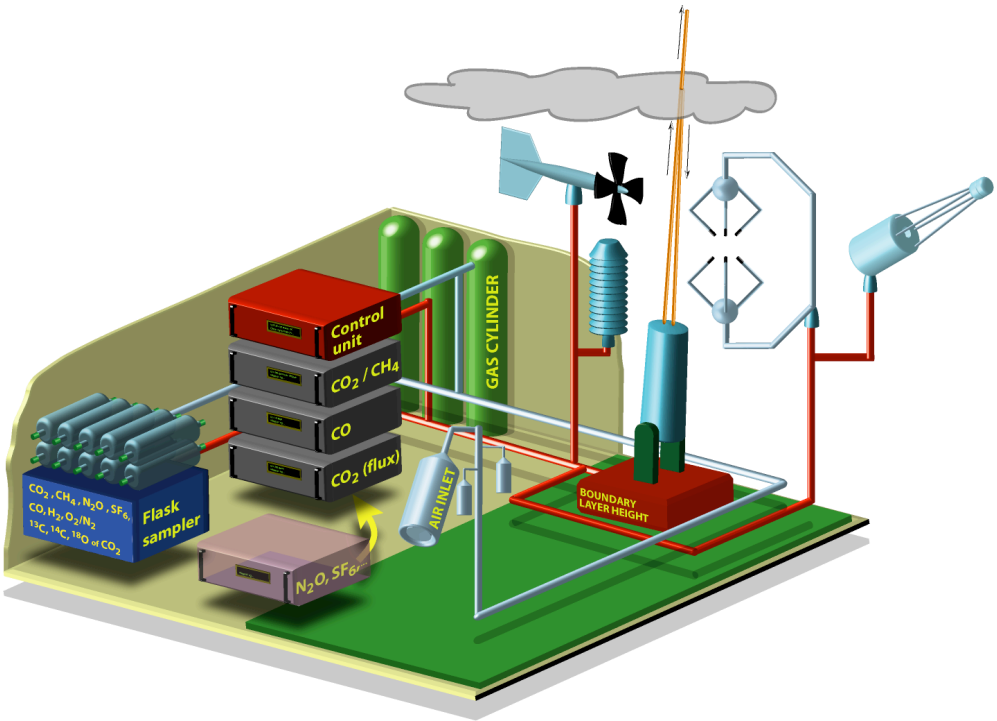

Figure 2 Conceptional drawing of the ICOS Atmospheric Station, which will be equipped with an automated flask sampling system, a weather station and different instruments to measure continuously GHGs and to determine planetary boundary layer height. (Used with permission from the illustrator Jošt V. Lavriče, 2008)

In order to manage the monitoring networks individually, three Thematic Centres (i.e. Ecosystem Thematic Centre, Atmospheric Thematic Centre, Marine Thematic Centre) will be set up (see Fig. 1). These Thematic Centres will provide different services to their corresponding network, such as technical and logistical assistance or testing of new instruments in close collaboration with research institutes and industry.

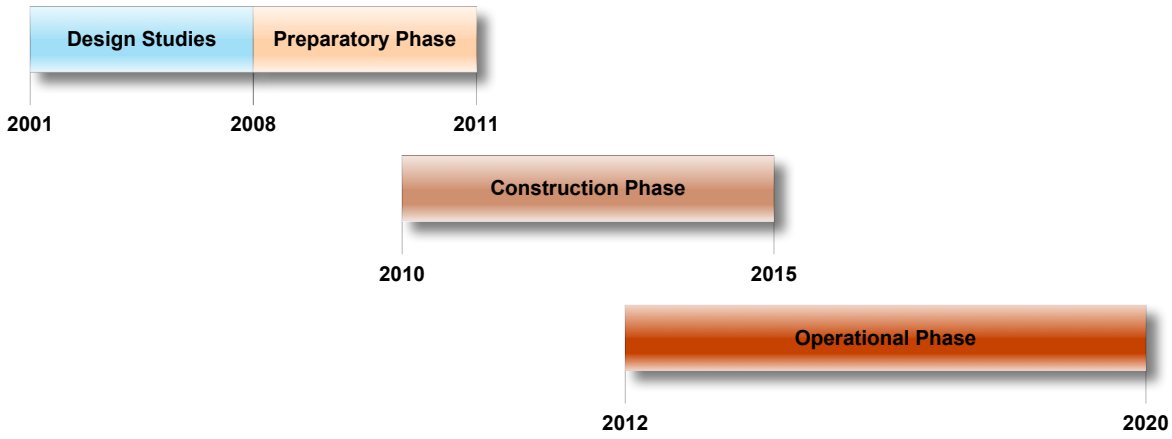

Figure 3 Implementation strategy of the ICOS project. (Illustration adapted from [18])

As illustrated in Figure 3 the implementation of ICOS will be realized in three stages. The preparatory phase, already started in 2008, will run till 2011. During this period, basic concepts will be developed concerning network design as well as equipment selection, testing and optimization. At the end of the starting phase the technical solutions will be developed up to a level of being fully operational for a six months test phase. The following construction phase will complete the deployment of the network and build and commission the central facilities. This part of the implementation is planned to enter between 2010 and 2011 in the different participating countries. ICOS is scheduled to run in an operational mode in 2012 and is expected to last for around 20 years. During its operational phase

greenhouse gas concentration and fluxes will be determined on a routine basis with operational costs of approximately EUR 14 million per year [20].

The establishment of an European integrated long-term research infrastructure will enable researchers a deeper understanding of the exchange of greenhouse gases and its driving forces over European countries. The construction of a dense atmospheric monitoring network will allow to determine fluxes of GHGs on a regional scale and to attribute them to processes as well as to detect small changes of greenhouse gas fluxes at an early stage. This will allow to estimate the effectiveness of European CO_2 mitigation efforts and could help to chart the accuracy of climate certificate systems that are currently in use in various European member states. Furthermore, emissions inventories of CO_2, based on calculations using industry and government data, can be independently verified by the precise atmospheric measurements of ICOS. In this way, ICOS will put Europe in a position to provide rigorously quality-tested data for long-term climate research and policy decision-making.

2.2 The ICOS Core Parameters for Periodic Flask Sampling

This section is concerned with the different species, that are planned to be obtained from weekly collected flask air samples at the ICOS AS. The gas species are described with respect to their contribution to the anthropogenic greenhouse effect. Atmospheric oxygen, as a relatively new species which is measured in flask samples, is also included since the gas serves as an additional indicator of global carbon cycle change. Finally, a brief overview about several isotopomeres in atmospheric carbon dioxide is given.

2.2.1 Carbon Dioxide

Carbon dioxide (CO_2) is a strong gaseous absorber of thermal infrared radiation in the atmosphere and serves therefore as an important determinant of the global heat balance of the earth-atmosphere system. After water vapor, the gas is the second-most contributor to the greenhouse effect and accounts for 63% of the total radiative forcing calculated for the major long-lived greenhouse gases [21].

Atmospheric CO_2 is closely related to biogeochemical processes in the terrestrial and marine systems, which involves the exchange of carbon among the individual compartments. These are for instance the dissolution of CO_2 into the oceans and in surface waters as well as the uptake by higher plants due to photosynthesis. In particular, due to the assimilation and respiration of the gas by the terrestrial vegetation, it is subjected to strong diurnal, seasonal and interannual variations that are most pronounced in the northern hemisphere. Nevertheless, the natural cycling of carbon is influenced by rising levels of atmospheric CO_2 associated with human activities which lead to an imbalance of the global carbon cycle and intensify the greenhouse effect, thus warming the Earth‘s climate [16].

Carbon dioxide emissions from fossil fuel burning and cement production are substantial and the dominant anthropogenic sources. Estimates from the Carbon Dioxide Information Analysis Center (CDIAC) show that global emissions of CO_2 from both sources had increased from approximately 3.2 Gt C in 1751 to 8.7 Gt C in 2008 [22, 23]. Additionally, changes in land use and land management, largely deforestation, lead to a loss of carbon from soils and plants. The global carbon flux to the atmosphere as a result from changes in land use is estimated to about 1.5 Gt C per year during the period from 2000 to 2005 [24]. As a consequence, the globally averaged atmospheric burden of CO_2 has increased since the pre-industrial era (taken as the year 1750 by the Intergovernmental Panel on Climate

Change (IPCC) [16]) from 278 ppm to 385 ppm in the year 2008 with an annual growth rate of approximately 2 ppm [23].

Since the first systematic measurements of atmospheric CO_2 in background air started in 1958 at Mauna Loa, Hawaii, the rising trend in atmospheric CO_2 levels is confirmed by numerous monitoring stations around the globe and there is a growing concern about the prospect of climatic changes if this trend continues. According to the IPCC Special Report on Emission Scenarios (SRES), projected atmospheric concentrations of CO_2 in 2100 are likely range from 540 to 970 ppm, compared to the pre-industrial value of 278 ppm [25].

2.2.2 Methane

Following carbon dioxide and water vapor, methane (CH_4) is the most abundant greenhouse gas in the atmosphere. It is a reactive trace gas, which is important to tropospheric and stratospheric chemistry. The gas is of special environmental concern since additional methane in the atmosphere is much more effective in absorbing infrared radiation than additional CO_2. Atmospheric concentration of CH_4 have been more than doubled since pre-industrial times. Referring to this, the globally averaged atmospheric mixing ratio of CH_4 increased from a pre-industrial value of 700 ppb to nearly 1,774 ppb in 2005 [16, 26].

Methane is released into the atmosphere from both natural and anthropogenic sources. Naturally emissions arise primarily from wetlands, termites, wild ruminants, oceans, hydrates and volcanoes. Anthropogenic sources can be distinguished into biogenic and non-biogenic sources. As a result from anaerobic decomposition of organic material by methanotrophic bacteria, anthropogenic emissions from biogenic sources are related primarily to waste disposal and agriculture (e.g. flooded soils in waste disposal sites, rice cultivation, domestic

ruminants, biomass burning). Main non-biogenic sources are leaks that occur during natural gas processing, transmission and distribution.

CH_4 is primarily removed from the atmosphere through the reaction with hydroxyl radicals (HO), accounting for about 90% of the global sink strength [26]. During the reaction formaldehyde and ozone (O_3) is formed provided that nitrogen oxides (NO_x) concentrations are above a threshold of 5-10 ppt [27]. It needs several chemical equations to describe the full reaction cycle of how CH_4 reacts with hydroxyl radicals (HO). Therefore, only the net equation (Eq. 2.1) is given [27].

$$\text{net: } CH_4 + 8O_2 + 5h\nu \rightarrow CO + 4O_3 + 2HO\bullet + H_2O \qquad (2.1)$$

Air samples, collected from sites in NOAA's Global Cooperative Sampling Network show that after a few years of a nearly steady global CH_4 budget, globally averaged atmospheric CH_4 started to increase again during 2007 and 2008 [28, 29].

2.2.3 Nitrous Oxide

Nitrous oxide (N_2O) is an atmospheric trace gas that plays an important role in the natural greenhouse effect and chemical processes in the stratosphere. Although it has a lower atmospheric concentration than CO_2 it is also contributing to the anthropogenic greenhouse effect due to its long atmospheric lifetime of around 120 years [30]. The contribution to the instantaneous radiative forcing by N_2O has increased from 5.9% in 1979 to 6.2% in 2004 [21].

With about 55% of the global total emissions of N_2O, most atmospheric N_2O is of biogenic origin [31]. Main natural sources can be found in soils (e.g. tropical and

temperate forests, grasslands) and aquatic systems, where the gas is produced by bacteria in nitrification and denitrification. Minor amounts of the gas are produced by chemical formation in the atmosphere.

As a result of human activities, global averaged mixing ratios of N_2O have been reached 322 ppb in 2005, which is considerably higher than the pre-industrial concentration of about 270 ppb [16, 30]. Because of the growing world population, the agricultural source (e.g. animal waste management systems) is nowadays the most important source of anthropogenic N_2O emissions, contributing about 34% to the global total emissions [31]. Above all, the use of synthetic fertilizers and animal manure results in an additional nitrogen availability for nitrification and denitrification in agricultural soils. Further nitrogen inputs (e.g. leaching and runoff from agricultural soils) into aquatic systems can also be associated with agriculture causing additional indirect emissions of N_2O. Further N_2O emissions are resulting from fossil fuel combustion, biomass burning, and the production of adipic and nitric acid, accounting 11% to the anthropogenic contribution to the global N_2O budget [31].

The main sink of N_2O is the stratosphere by degrading the gas through photodissociation which causes a depletion of O_3. The average loss rate of N_2O in the stratosphere has been estimated to 16.5 Tg per year [32]. In spite of the fact that N_2O is the dominant ozone-destroying compound emitted from human activities, it is not regulated by the Montreal Protocol [33].

2.2.4 Sulphur Hexaflouride

Sulphur hexaflouride (SF_6) is one of the most potent greenhouse gases and is mainly anthropogenic in origin. The main feature, which has brought the gas into the climate impact discussion is its extremely high atmospheric lifetime, estimated

as 800 to 3200 years, and its large global warming potential (GWP100), which is 23,900 times greater than that of CO_2 [16].

With a small natural background of 0.054 ppt, SF_6 does not have significant natural sources [34]. Primary emissions of the gas are produced by the electric power industry, where it is preferably used in gas-insulated equipment for electrical transmission and distribution systems (e.g. in gas insulated switchgear). Furthermore, it is used in blanketing or degassing of molten reactive metals such as magnesium and aluminium. Due to its well understood sources, it is also deliberately emitted as an inert tracer in order to study atmospheric and oceanic transport processes [34].

Atmospheric measurements reveal that the global mean surface concentration of SF_6 has increased from 0.6 ppt at the beginning of 1978 up to 6.7 ppt by the end of 2008 [16, 35]. To date, the use of the gas is widespread and production is steadily growing leading to an annual growth rate of approximately 7% [36].

2.2.5 Carbon Monoxide

There are several gases, which do not have a direct radiative impact on the atmosphere since they do not absorb terrestrial infrared radiation strongly enough. However, these gases act as indirect greenhouse gases by influencing the formation and destruction of tropospheric and stratospheric O_3 and other GHGs. Besides non-methane hydrocarbons (NMHCs), carbon monoxide (CO) is one of the most important indirect greenhouse gases. CO is the main reaction partner for HO radicals. Therefore, HO levels are often controlling the concentration of tropospheric CO directly. A lot of natural and anthropogenic gases are also removed from the atmosphere through HO radicals, in particular CH_4. Hence, the cycle of CO itself cannot be uncoupled from global cycles of other GHGs.

Furthermore, the chemical reaction of CO with HO radicals produces considerable amounts of tropospheric O_3 and CO_2 depending on levels of NO_X [27]. In this way, increasing emissions of CO in the atmosphere have a significant indirect impact on the global climate.

Main anthropogenic emissions of carbon monoxide are resulting directly from the combustion of fossil fuels and biomass, which is more than 70% of the total CO budget produced by human activities. The rest is attributed to the oxidation of industrial hydrocarbons. On the other side, oxidation of natural produced CH_4 and NMHCs can be considered as the main natural source, contributing almost 85% to the natural source budget. Other natural sources are the oceans and vegetation [37].

As mentioned above, the reaction of HO provides a major sink process for removing CO from the atmosphere, accounting 90-95% of the global CO sink strength (see Eq. 2.2 & 2.3) [38]. Further reduction of the gas occurs through soil deposition and by diffusion into the stratosphere.

$$CO + HO\bullet \rightarrow CO_2 + H\bullet \tag{2.2}$$

$$H\bullet + O_2 + M \rightarrow HO_2\bullet + M \tag{2.3}$$

Starting from Equation 2.2 and 2.3, CO also impacts the formation of O_3 in regions with high NO_X levels (see Eq. 2.4) [27]. Conversely, in regions of low NO_X concentrations, HO_2 radicals produced from oxidation of CO, react directly with O_3 which leads to a net ozone destruction (see Eq. 2.5) [27].

$$\text{net: } CO + 2O_2 + h\nu \rightarrow CO_2 + O_3 \tag{2.4}$$

$$\text{net: } CO + O_3 \rightarrow CO_2 + O_2 \tag{2.5}$$

The average lifetime of CO is about two month, which is short enough to cause large spatial variation within the lower troposphere. The distribution of CO in the lower troposphere has also been determined from flask measurements since 1988 as part of the NOAA/ESRL Cooperative Flask Sampling Network. Based on this observations, CO mixing ratios are varying from 200-225 ppb in the northern hemisphere down to 35-40 ppb in the southern hemisphere [38]. Periodic and event-based sampling have also demonstrated that CO can serve as a quantitative tracer for anthropogenic emissions of CO_2 from fossil fuel and biomass burning [11, 14].

2.2.6 Hydrogen

Molecular hydrogen (H_2) is an important trace gas of stratospheric and tropospheric chemistry and its biogeochemical cycle is closely coupled to the atmospheric cycles of CH_4 and CO. Flask measurements obtained from NOAA's air sampling network show a globally averaged H_2 mixing ratio of 531 ppb [39]. This is more than twice in contrast to the estimated concentration of 200 ppb before the beginning of the industrial revolution [40].

The global budget of tropospheric H_2 is comprised of four main sources which are accountable for nearly 90% of the total emissions [39]. These are photochemical sources characterized by the oxidation of CH_4 and NMHCs and the combustion of fossil fuels and biomass whereby anthropogenic sources are predominantly related to combustion activities. The remaining 10% can be attributed to emissions from minor sources, for instance volcanoes, oceans or nitrogen (N_2) fixation by legumes [39].

Primarily sinks for H_2 are the oxidation of HO in the sunlit troposphere and the biologically driven uptake by soil. Especially the reaction with tropospheric HO

radicals perturb the distribution of methane and ozone, the most important greenhouse gases after CO_2. Therefore, increasing levels of H_2 may indirectly affect the global climate, which might be of particular interest concerning to the prospect of a future H_2 fuel economy.

2.2.7 Oxygen

Measurements of atmospheric CO_2 concentration are very important in every respect since the gas is a key player in causing changes in the Earth's climate system. Terrestrial and oceanic reservoirs for CO_2 uptake are very heterogeneous. Therefore, it is very difficult to estimate oceanic and land biotic carbon sinks only by measuring background CO_2 in the atmosphere. Thus, several other methods have been established to quantify the partitioning of CO_2 through gas exchange between atmosphere and terrestrial biosphere/oceans. One of these methods is the use of high precision atmospheric oxygen (O_2) measurements, earlier described and expanded by R. Keeling [41, 42].

Fractional changes in O_2 concentration are very small and superimposed on its large atmospheric background of nearly 21%. Based on its high abundance, it is not possible to indicate observed changes in O_2 concentration as an absolute value. Consequently, changes in O_2 concentration are measured relatively to an arbitrary chosen standard, and reported as O_2/N_2 ratios in units of per meg (see Eq. 2.6) [43].

$$\delta(O_2/N_2) = \left[\frac{(O_2/N_2)_{\text{Sample}}}{(O_2/N_2)_{\text{Reference}}} - 1 \right] \cdot 10^6 \qquad (2.6)$$

The unit per meg can be converted in ppm by multiplying the standard oxygen mole fraction of dry air, according to Machta and Hughes, with the mixing ratio in per meg [44]. This relationship is given in Equation 2.7.

$$\frac{1\ \text{ppm}}{0.20946} \approx 4.8\ \text{per meg} \tag{2.7}$$

Variations of the atmospheric oxygen content are inversely coupled to changes in atmospheric CO_2 and primarily induced by fossil fuel combustion, respiration, photosynthesis and gas exchange between the atmosphere and the oceans. Apart from the oceanic O_2 sink, terrestrial processes can be distinguished from each other through their different O_2/CO_2 molar exchange ratios. The actual O_2/CO_2 molar ratio for photosynthesis and respiration is approximately 1.1 and can be represented with Equation 2.8 [42].

$$CO_2 + H_2O \rightarrow CH_2O + O_2 \tag{2.8}$$

Atmospheric O_2 is also consumed by fossil fuels and biomass burning, which can be described stoichiometrically according to Equation 2.9, where the molar exchange ratio O_2/CO_2 is depending on the composition of the fossil fuel. The global average O_2/CO_2 exchange ratio for fossil fuel is 1.4 [42].

$$CH_X + (1 + \frac{1}{4}X)O_2 \rightarrow CO_2 + \frac{1}{2}XH_2O \tag{2.9}$$

Differences between atmospheric CO_2 and O_2 in the exchange through the air-sea interface and the storage in seawater allow an additional separation between both gases. CO_2 reacts with seawater to carbonic acid, bicarbonate and carbonate ions.

Therefore, the solubility of CO_2 is much greater than the solubility of O_2. To give an example, the solubility coefficient for CO_2 calculated for 24 °C water in the Western Pacific is six hundred times greater than the solubility coefficient for O_2 [41]. In addition, the equilibration rate for both gases is different. Surface waters tend to equilibrate with the atmosphere roughly ten times faster for O_2 than for CO_2. Furthermore, one have to take into account that only 1% O_2 in the ocean-atmosphere system is in the ocean, and there is no significant O_2 flux from the oceans counterbalancing the corresponding decrease of atmospheric O_2 through fossil fuel combustion. On the other hand, rising atmospheric levels of CO_2 drive a CO_2 flux into the oceans and perturb the atmosphere-ocean equilibrium [9].

The first O_2 measurements using a flask sampling network started in 1989 under the guidance of R. Keeling at the Scripps Institution of Oceanography (San Diego, USA). Regular measurements from the Scripps atmospheric oxygen flask sampling network show a very similar trend in the annual decrease of atmospheric O_2 concentration which amounts to 19 per meg per year [9].

2.2.8 Isotopic Signatures in Carbon Dioxide

Analyzing atmospheric CO_2 for its isotopic ratios provides an important source of additional information for global carbon cycle research. The carbon cycle is characterized by an active exchange of CO_2 among the atmosphere, terrestrial biosphere and the surface ocean. The processes responsible for circulating CO_2 within the carbon cycle (e.g. fractionation, mixing, radioactive delay) lead to characteristic isotope patterns through distributions in the organic and inorganic carbon reservoirs [45]. In this context, studies of isotope ratios of atmospheric CO_2 can be used to distinguish fluxes between atmosphere and ocean from those between atmosphere and terrestrial biosphere. Furthermore, it forms the basis for

partioning the measured CO_2 mixing ratio into a biospheric, a fossil and a background component. It is therefore a common strategy to supplement CO_2 mixing ratio measurements by isotopic analysis. Table 2.1 presents a survey of isotopes in atmospheric CO_2, which will be covered by the ICOS analysis strategy.

Table 2.1 Isotopes in atmospheric CO_2 which will be covered by the combined ICOS CO_2 concentration measurements: properties, international standards and natural abundances.

	^{12}C	^{13}C	^{14}C	^{16}O	^{18}O
stability	stable	stable	radioactive	stable	stable
natural abundance	0.989	0.011	$< 10^{-12}$	0.9976	0.00205
standard		VPDB*	oxalic acid II		VPDB*

*Vienna-PeeDee Belemnite

For most natural samples, variations in the isotopic ratio are very small, usually in the range of the third to fifth decimal place. Thus, isotope measurements are made relative to the isotopic ratio of a reference standard and commonly expressed in δ values in units of per mill (see Eq. 2.10) [45].

$$\delta^{H}X = \left[\frac{R_{Sample}}{R_{Standard}} - 1\right] \cdot 10^{3} \qquad (2.10)$$

Carbon exists in two stable isotopic forms, ^{12}C and ^{13}C. Differences in $\delta^{13}C$ signatures between the several compounds of the global carbon cycle (i.e. fossil fuels, vegetation, soils, oceans) are particularly useful for measuring fluxes, and to distinguish between various CO_2 sink processes. In general, more negative values are observed in continental air because of an admixture of CO_2 of anthropogenic

and biospheric origin since CO_2 from vegetation, soil and combustion of fossil fuels is depleted in ^{13}C. On the contrary, higher values can be found in air remote from terrestrial influences, typically at oceanic sites [46].

A mass spectrometric $\delta^{13}C$ analysis of CO_2 delivers a $\delta^{18}O$ result as well, which can be useful to estimate land biosphere activity. Differences in $^{18}O/^{16}O$ ratio depends critically on the isotopic composition of the water in which atmospheric CO_2 is dissolved. As a result, $\delta^{18}O$ signals of atmospheric CO_2 are dominated by the $\delta^{18}O$ imprint of both precipitation and ocean water, which is caused by the oxygen isotope exchange through formation of carbonic acid. Furthermore, on a local scale, measurements of $^{18}O/^{16}O$ are an important tool to distinguish between changes in the rates of plant photosynthesis versus plant respiration since the same effect is present in leaves and roots [47]. However, the process of isotopic exchange, that may occurs in the flask sample treatment, can cause additional experimental problems [48].

Unlike ^{12}C, ^{13}C, ^{16}O and ^{18}O, radiocarbon (^{14}C) is not stable and undergoes a natural radioactive decay in $^{14}NO_2$ with a half-time of 5730 years according to Equation 2.11-2.14. Natural ^{14}C is mainly produced by interaction of cosmic ray associated with the production of neutrons at the stratospheric level [27].

$$^{14}_{7}N + {}^{1}_{0}n \rightarrow {}^{14}_{6}C + {}^{1}_{1}H \tag{2.11}$$

$$^{14}_{6}C + O_2 \rightarrow {}^{14}_{6}CO + O \tag{2.12}$$

$$^{14}_{6}CO + HO\bullet \rightarrow {}^{14}_{6}CO_2 + O \tag{2.13}$$

$$^{14}_{6}CO_2 \rightarrow {}^{14}_{7}NO_2 + \beta \tag{2.14}$$

Anthropogenic ^{14}C is primarily based on the releases of $^{14}CO_2$ by nuclear power plants and detonations of nuclear warheads and are superimposing the natural ^{14}C

signal. In particular, extensive atmospheric nuclear bomb tests in the 1950s and early 1960s lead to a global increase in the $^{14}C/^{12}C$ ratio of atmospheric CO_2 and a substantial disequilibrium of ^{14}C between atmosphere, biosphere and surface ocean water [49].

One of the main advantage to use atmospheric ^{14}C in studies of climate change is based on the Suess effect, meaning that an increasing input of ^{14}C-free fossil fuel CO_2 causes a corresponding dilution of ^{14}C in the atmosphere [50]. Thus, the regional fossil fuel CO_2 can be calculated from $^{14}CO_2$ observations at a polluted sampling site if the undisturbed background $^{14}CO_2$ level is given [51]. Furthermore, ^{14}C records can be used as an input function for global carbon cycle models for tracing transport pathways and associated timescales [49].

2.3 Description of the Automated Air Sampling System

The automated air sampling system, which will be described in this chapter, was purchased from the North American company High Precision Devices Inc. (Boulder, USA). It comprises of a Programmable Flask Package (PFP) and a Programmable Compressor Package (PCP). The system was developed by the Climate Monitoring and Diagnostic Laboratory (CMDL) of the National Oceanic and Atmospheric Administration (NOAA; Boulder, USA) with the main objective to acquire air samples from aircraft more efficiently. Previous models of the sampler have been used by NOAA since 1994 and the basic configuration as well as the necessity of such a system was already described in 1996 by Tans et al. [52]. Along with the expansion of their vertical profile network, NOAA intensified the usage and further development of automated whole air samplers as well [53]. Updated models of the air sampling system are in use for several ongoing flask

sampling campaigns, such as for the NOAA CMDL aircraft sampling program for vertical profile measurements or the weekly airborne carbon measurements of the ARM Climate Research Facility (ARM-ACME) in the Southern Great Plains (USA).

2.3.1 The Programmable Compressor Package

The Programmable Compressor Package (PCP) is one of the major components of the automated air sampling system. It is enclosed in a foam-lined black suit-case and is used in conjunction with the Programmable Flask Package. It has the main task to provide a filtered, dried flow of pressurized sample air to the flask package. For that purpose, the PCP is equipped with two diaphragm pumps, which are connected in series to act as a two-stage compressor (model N811 & N828, KNF Neuberger, Trenton, USA), a thermoelectrical cooler (see Sec. 2.3.3) and two micron particle filters (SS-4FW4-2, Swagelok, Solon, USA). The unit also contains a rechargeable battery pack (HHR380A, Panasonic, Secaucus, USA) to operate the system without constant power supply, for instance at sampling sites with lacking infrastructure. Furthermore, it is equipped with a mass flow meter (AWM5104VN, Honeywell, Minneapolis, USA) at the sample air inlet and a pressure transducer (19C100PA4K, Honeywell, Minneapolis, USA) at the outlet for integral flow and pressure sensing. The PCP provides the sample air flow through a flexible stainless steel hose to the Programmable Flask Package. The entire system is illustrated in Figure 5, which shows the whole air sample flow path and substantial components of the package.

The PCP can be configured by connecting a terminal emulator to the RS-232 serial interface. By accessing specific single-character commands, the user is able to calibrate the sensors, test pump operation and specify pressure limits. In

contrast to the PFP, the PCP does not require any additional programming before a sampling cycle can start.

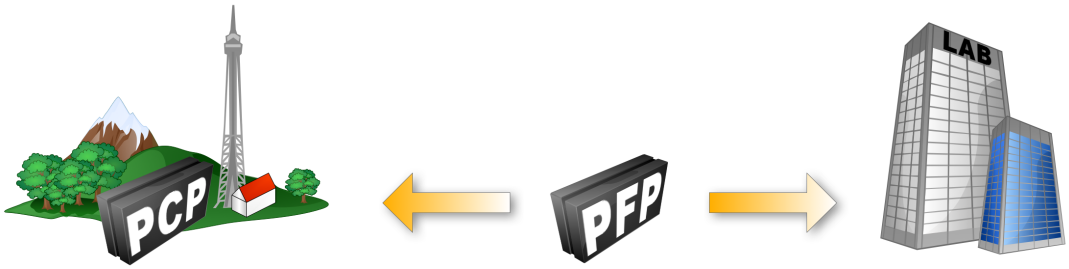

Figure 4 Typical application of the PCP/PFP using tall tower installation as an example. Only the flask package is shipped. The compressor package remains at the sampling plot.

The Programmable Compressor Package is usually intended to be kept at the air sampling site after all samples are taken, whereas the PFP is shipped to the sampling site and central analysis facility. This scenario is illustrated in Figure 4.

2.3.2 The Programmable Flask Package

The second major component of the air sampling system is the Programmable Flask Package, fully illustrated in Figure 5. It is a suitcase mounted multi-flask array, containing twelve borosilicate glass flasks (Glass Expansion, Melbourne, Australia), which are fitted in a subassembly of polycarbonate (Lexan®) tubes. The flasks have a nominal volume of 0.7 L and are connected in parallel through a flexible stainless steel manifold (m009-02, HPD, Boulder, USA). The ends of each flask narrow into valves and are sealed with PTFE O-rings. In order to open and close the valves automatically, each valve is equipped with a piston (m009-16, HPD, Boulder, USA), which is linked through a gearwheel to a servo-motor (A-max 16 with planetary gearhead GP 16 A, Maxon, Sachseln, Switzerland). Additional Lexan® tubes are containing a microcontroller, a solenoid valve

(B14DK1030, Parker, Cleveland, USA) and a pressure transducer (19C100PA4K, Honeywell, Minneapolis, USA). Both sensor and solenoid valve are placed at the end of the air sample flow path, whereby the alve helps to create the desired overpressure in the sample containers (see Fig. 5).

In order to configure and program the PFP as well as to retrieve additional information after sampling procedure is completed (e.g. fill pressure, flush volume) the PFP is equipped with a RS-232 serial host port. This allows one, similar to the PCP, to communicate with the internal controller by using a simple terminal emulator. In this way, the PFP can be programmed to acquire air samples at predetermined times, altitudes and locations, if a GPS receiver is attached to the system.

Table 2.2 Three methods of triggering a sample: fully-automatic, semi-automatic and manual.

Sampling	Features	Typical application
fully-automatic	Sampling will be initiated when conditions (e.g time) are matching with those from the pre-programmed sampling plan.	*stationary installation at remote sites*
semi-automatic	Samples can be taken at any time by using the Pilot Display but programmed values will be still considered.	*aircraft installation*
manual	Flasks can be filled (and unloaded) at any time through different serial commands.	*package preparation, maintenance, flask analysis*

A sample cycle can be triggered in different ways, depending on the conditions, which under the sampling system is operating. Table 2.2 shows the main operational modes of the PFP and their typical application. Each method of triggering sampling has advantages and disadvantages. Above all, using the PFP

in fully-automatic mode is most suitable for unattended sampling at remote sites and for campaigns where manpower for sampling processing is a limiting factor. However, this method has one distinct disadvantage. That is, supposing that a given sample cannot be triggered for some reason, then none of the following samples can be triggered. This perturbing fact can be circumvented by using the Pilot Display (see Fig. 7 in Sec. 2.3.4). In this way, flask filling can be initialized by pushing a switch on the display device, irrespective of the pre-programmed sample plan.

Nevertheless, in case of operating the system in one of the automatic modes samples are taken in order, starting with the first flask until all available flasks are filled. After the whole sampling cycle is completed, it is not possible to restart the sample plan again. Therefore, the manual sampling mode allows a maximum flexibility in sampling, since every flask can be filled and refilled individually without programming the PFP. This is also the preferred method to unload flasks for introducing air samples into the analytical system.

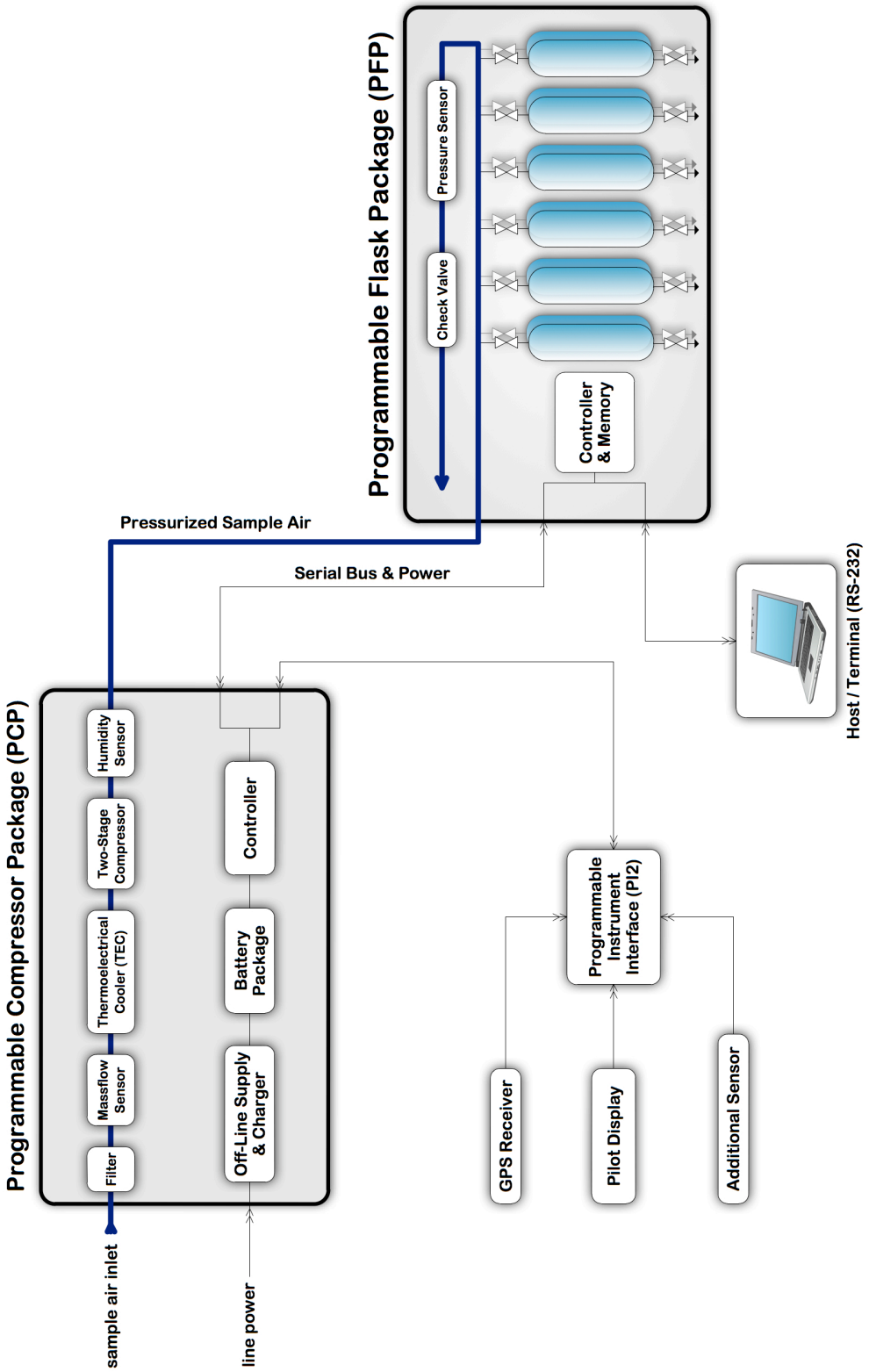

Figure 5 System overview of the automated flask sampling system. (Adapted from the illustrator Doug Ghuenter, 2001)

2.3.3 The Air Sample Dryer

The main function of the air sample drying system (see Fig. 6) is the removal of moisture from the air sample stream which is being compressed into the flasks. The drying system is based on the principle of thermoelectric refrigeration and integrated in the PCP. It consists of eigth Peltier modules (SH10.125.05.L1.RTW.W18, Laird Technologies, Chesterfield, USA) divided into two channels, cooling fans, heat sinks (p03115-153-0, High Precision Devices Inc., Boulder, USA) and an electronic controller module (CryoController, Science Circuit Designs, Bozeman, USA) for power modulation.

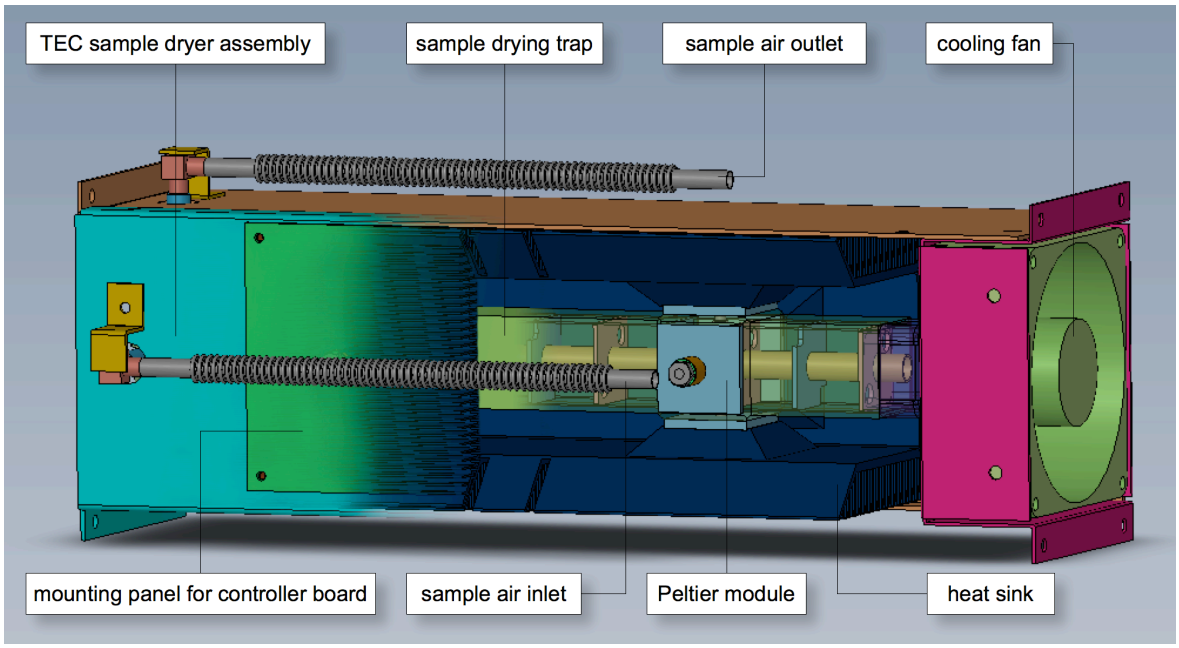

Figure 6 Cross section of the integrated air sample drying system. (Used and modified with permission from High Precision Devices Inc., 2009)

Dehumidification of the air sample stream is achieved by cooling the inner surface of the dryer tube below dew point temperature of the sample air. If sample air passes the cooled surface, the containing water vapor is separated through

freezing. The dried sample air exits the drying trap through an inner tube to the two-stage compressor. The sample drying trap is divided into numerous chambers in order to ensure that the sampled air is well mixed and resides in the dryer channel as long as possible. An additional sensor for measuring relative humidity (HIH-3602-L IC, Honeywell, Minneapolis, USA) is installed at the end of the sample air outlet. The trapped water is removed through evaporation which is achieved by reversing the polarity of the Peltier modules.

It is necessary to point out that the thermoelectrical cooler (TEC) was still in development when the work on this thesis began. It is not fully tested by NOAA's research department and therefore not applicable to run under field conditions. One of the restriction is that there is no communication between the dryer system and the PCP. Therefore, the thermoelectrical cold traps cannot be operated automatically by the PCP internal controller. For controlling the dryer while the PFP/PCP is running, the electronic controller module has to be connected to a serial port through an RS-485 interface. A set of serial commands can be used to control the cooling elements and fans of the TEC hardware. Thus, bench testing is the only possibility to handle important operating modes like sample drying and trap drying. The minimum temperature that can be achieved by the dryer is around -12 °C at a sample flow rate of 15 L min^{-1} (B. Hollander, personal communication, September 4, 2008).

2.3.4 Additional Equipment

As mentioned above, it might be advantageous to trigger sampling in semi-automatic mode through the Pilot Display interface (see Fig. 7). As the name already suggests, the Pilot Display is usually used at small aircraft where it can be located on the dashboard, within reach of the pilot. After the device is plugged

into the remaining connector on the PFP, the next pre-programmed sample can be taken by pushing the momentary switch.

Figure 7 The Pilot Display, which is required for semi-automatic sampling.

Depending on the individual requirements of the sampling campaign, additional data might be necessary to characterize sampling events more precisely. For that purpose, additional sensors can be attached to the system by using the Programmable Instrument Interface (PI2) (see Fig. 8).

Figure 8 The Programmable Instrument Interface.

The PI2 is a serial communication device, interfacing directly with the PFP. It includes additional serial ports that can be used to connect other serial instruments, for instance a temperature/humidity probe or a GPS receiver. Furthermore, the PI2 contains an onboard pressure transducer (MS5534B, Interserma, Bevaix, Switzerland) for absolute pressure measurements.

Chapter 3

Enhancements and Experiments

This chapter contains the detailed description of the laboratory tests that were performed at MPI-BGC in order to investigate the influence of instrumental factors and to better characterize the system performance of the automated flask sampling system. Furthermore, the enhancements are described that were necessary to meet specific requirements of the future ICOS flask sampling program. Experiments and improvements are reported in the order as they have been carried during the work on this thesis. Section 3.1 describes a method that makes it possible to retrofit the flasks in the PFP with commercially available PCTFE seals to improve their storage characteristics. Section 3.2 is concerned with the experimental investigation of memory effects and section 3.3 reports the results of an intercomparison experiment that was performed in conjunction with a cavity ring-down analyzer.

3.1 Improving Flask Sample Storage Characteristics

3.1.1 Preliminary Consideration

Apart from choosing appropriate filling procedures, it is also important to select suitable flask materials. Flasks for atmospheric air sampling are commonly made

of glass and sealed with a polymer material. Since the sealing should prevent the loss of sample air during flask storage, the effectiveness of the seal is particularly crucial to the sample integrity. Nevertheless, even without a leakage the composition of atmospheric air collected in glass flasks can be altered by several processes due to the use of polymer seals. These are for instance permeation, physical adsorption, outgassing effects (e.g. water vapor, plasticizers, inhibitors) and even oxidation of grease, which is sometimes used to lubricate seals. Especially, the permeation of individual gas components through elastomeric seals can deteriorate the sample quality, provided that a partial pressure between sample and surrounding air exists [54]. Effects of permeation can become more significant when samples are exposed to long storage periods, which can occur due to logistical problems in sample transport, for instance from remote sites or if analysis capacities are exhausted. Above all, for measurements like $\delta(O_2/N_2)$ where highest attainable precision is needed, permeation might cause large systematic errors in the analysis results.

$$Q_P = K(T) \cdot \frac{A}{d} \cdot \Delta p \tag{3.1}$$

The rate at which a gas permeates through a polymer material can be described as a three-step process. At first, the gas gets absorbed into the polymer. After the permeant has passed the polymer matrix by diffusion towards the lower pressure side, it finally desorbs into a pure gas stream. A simplified description of the permeation flux Q_P of a gas, which is exposed to a partial pressure difference Δp, through a material with given material thickness d and surface area A is given by Equation 3.1.

To emphasize the risk of altering the sample air during storage through permeation, Table 3.1 shows the calculated permeation flux Q_P of some atmospheric

gases through two O-rings constructed from polychlorotrifluoroethylene (PCTFE) and polytetrafluoroethylene (PTFE). Material thickness and surface area are referring to the dimensions of the O-rings, which are used to seal the flasks in the PFP. The results indicate that the rate of Q_P is the smallest for PCTFE, which is primarily related to its lower permeation coefficients. In particular, the degradation of O_2 and N_2 after a one year storage period can be reduced about three orders of magnitude if PCTFE is used for flask enclosure instead of PTFE.

Table 3.1 Permeation of CO_2, O_2 and N_2 through two PTFE/PCTFE O-rings for a pressure difference of 1 bar between ambient and flask pressure. Dimensions based on the O-rings in the 0.7 L flasks: Thickness d = 0.18 cm and area A = 0.33 cm^2 (D. Senders, personal communication, November 7, 2009).

Polytetrafluoroethylene (PTFE)			
Gas	K(T)* $cm^2\ bar^{-1}\ s^{-1}$	Q_P $cm^3\ s^{-1}$	Q_P after one year cm^3
CO_2	$7.51 \cdot 10^{-8}$	$2.02 \cdot 10^{-10}$	$6.371 \cdot 10^{-3}$
O_2	$3.37 \cdot 10^{-8}$	$4.996 \cdot 10^{-8}$	1.575
N_2	$1.44 \cdot 10^{-8}$	$7.959 \cdot 10^{-8}$	2.510
Polytetrafluoroethylene (PCTFE)			
CO_2	$0.04 \cdot 10^{-8}$	$1.076 \cdot 10^{-12}$	$3.393 \cdot 10^{-5}$
O_2	$0.02 \cdot 10^{-8}$	$2.965 \cdot 10^{-10}$	$9.352 \cdot 10^{-3}$
N_2	$0.004 \cdot 10^{-8}$	$2.211 \cdot 10^{-10}$	$6.972 \cdot 10^{-3}$

*Permeability values from [55, 56] .

It has to be said that the permeation coefficient K(T) in Equation 3.1 is not a fundamental property of a polymer. It is usually obtained from a standard test, but also from other measurement methods than standard procedures [57]. Hence,

different measurement methods and purposes in investigation are lead to a wide range of uncertainties in reported permeation coefficients. Additional influences, for instance variations in material composition and changes in temperature and cross section of the O-ring during use cannot be considered by assessing permeation rates with Equation 3.1.

Flask storage tests performed at the MPI-BGC have already proven that using seals constructed from PCTFE can substantially reduce the loss of air caused by permeation [58]. For that reason, Brand et al. developed in collaboration with Normag GmbH (Ilmenau, Germany) a PCTFE-on-glass seat for sealing 1 L glass flasks that are used for regular flask sampling activities within the MPI-BGC Tall Tower Network [59]. Owing to its greater hardness PCTFE is not suitable to apply it as a simple O-ring, which is a common method of sealing flasks for air sampling where the O-ring is mounted in a notch on a glass shaft. Due to this, the PCTFE seal is designed as a cap and fixed at the end of a glass plug (see Fig. 9). Besides minimizing effects of permeation, another advantage of this glass stopper is its compatibility to flask types from Glass Expansion Inc. with which the PFP is equipped by default.

For aforementioned reasons it is necessary to equip the flasks in the PFP with PCTFE seals. This will ensure to obtain more reliable flask data from the future ICOS flask sampling network with the here evaluated flask sampling system. The following section describes the technical approach to retrofit the 0.7 L flasks in the PFP with commercially available PCTFE seals.

3.1.2 Material and Methods

Replacing the PTFE flask seals with the above described PCTFE-on-glass seats demands an adjustment of the pistons, which are threaded on the flasks. In order

to insert the improved glass stopper into a piston, a cylindrical cut out was drilled into the center of each piston by using a lathe. The depth of the drill-hole has been chosen in such a manner that the position of the PCTFE sealing cap is consistent with those of the PTFE O-ring. In addition to this, a groove was cut into the bore in order to fasten the glass plugs by installing an internal retaining ring (DHO DIN 472, Rotor Clip, Idstein, Germany). This technique was chosen, because retaining rings provide a more simple and cost-effective solution in contrast to traditional fasteners, such as screws. The distance between the shoulder of the retaining ring and the top of the glass plug provides sufficient space that a glass stopper does not rotate when a piston is threaded on a flask. Otherwise, glass shafts are subjected to high torsional stress during valve opening and closing and tend to break off. The customized piston is illustrated in Figure 10.

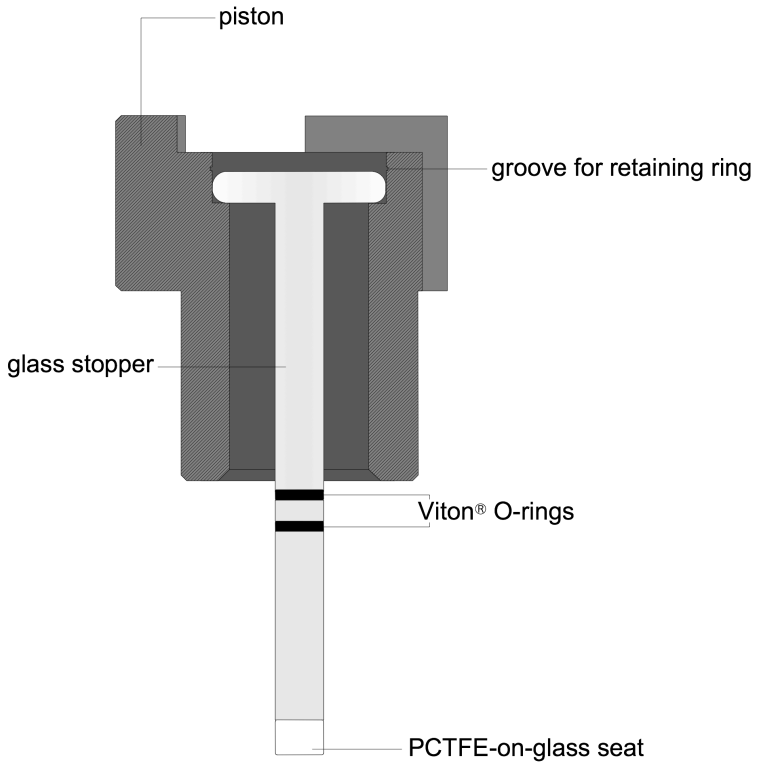

Figure 9 The customized piston, which suitable for the installation of glass stoppers from Normag GmbH. The glass stopper is equipped with two Viton® O-rings and a PCTFE sealing cap.

3.1.3 Laboratory Test

A leakage test was performed to investigate if significant diffusion of sample air around the seal can be occur. One way for determining a leakage is to use the pressure decay method. The pressure decay method, from literature also known as “back pressurizing“, involves a test vessel, which is subjected to a pressurized gas. After the vessel is closed the pressure is monitored, whereby any decrease in air pressure over time signifies a leak [60].

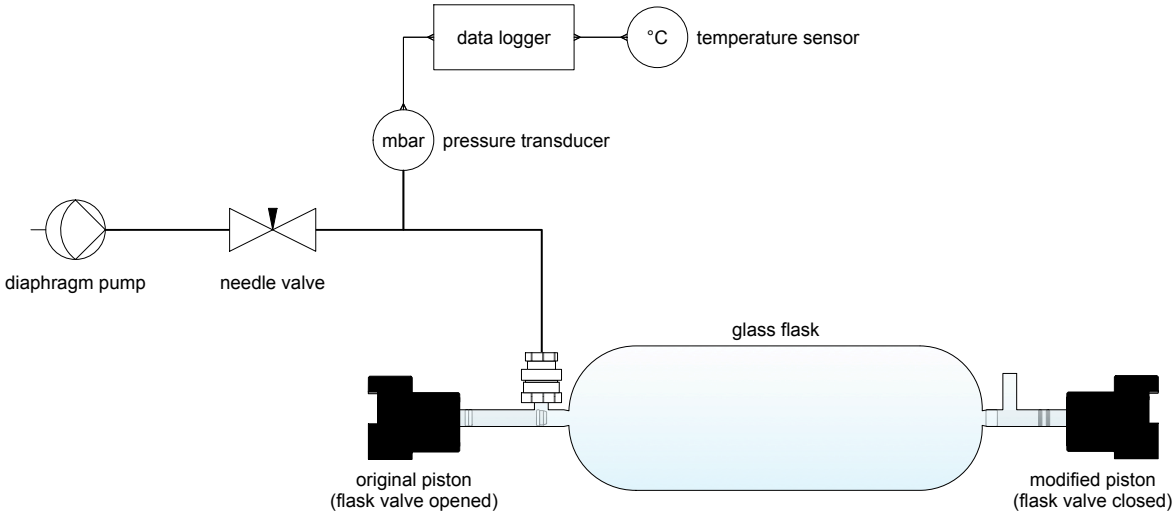

Figure 10 Experimental setup for pressure-decay leak testing in a 0.7 L glass flask. A diaphragm pump was used to pressurize the flask. After the system was closed with a needle valve, pressure and temperature were recorded with a data logger.

The experimental setup is illustrated in Figure 10 and the test was performed as follows: The 0.7 L glass flask was connected to a supply line (1/4“ OD, Synflex, Saint-Gobain, Courbevoie, France) using an Ultra-Torr Vacuum Fitting (SS-6-UT-1-4, Swagelok, Solon, USA) and filled with ambient air. The air flow was drawn through a needle valve (SS-SS4, Swagelok, Solon, USA) by means of a diaphragm pump (N811 KNDC, KNF Neuberger, Freiburg, Germany). After a

flask inlet pressure of approximately 2 bar was reached, the needle valve was closed and the pressure was measured using an absolute pressure transducer (CTE7005AM7, Sensortechnics, Puchheim, Germany). Furthermore, a temperature sensor (107-L, Campbell Scientific, Logan, USA) was installed to compensate the results for temperature-induced pressure-change effects. Both temperature and pressure were recorded with an external data logger (CR23X, Campbell Scientific, Logan, USA). Nevertheless, with this experimental setup it is not possible to conclude that a pressure decay is solely caused due to an insufficient compression of the PCTFE seal because only the leakage of the total system can be detected.

3.1.4 Results

Figure 11 shows the steady decrease in flask pressure over a test period of 12 days indicating a loss of sample air in the flask through leakage. The curve is representing the temperature compensated pressure values obtained from Equation 3.2. In Equation 3.2 is p the measured system pressure and T the ambient temperature. T_0 is the reference temperature after the flask volume had stabilized. The stabilization phase is particularly crucial since the pressurized air will cool by dissipating adiabatic heat which was generated because of the compression of the test gas. The period in which the flask was pressurized and the stabilization phase are not shown in Figure 11.

$$p_{corrected} = p \cdot \frac{T_0}{T} \tag{3.2}$$

Based on the difference between initial (2031.07 mbar a) and end pressure (2030.29 mbar a) in the decay curve the leak rate Q_L for the given system volume V (0.7 L) and test interval Δt (~12 days) can be calculated according to Equation 3.3.

$$Q_L = V \cdot \frac{\Delta p}{\Delta t} \tag{3.3}$$

Considering that sample air passes through two valves, the leak rate in the glass flask is twice as Q_L and amounts to $1.04 \cdot 10^{-6}$ L mbar s^{-1}.

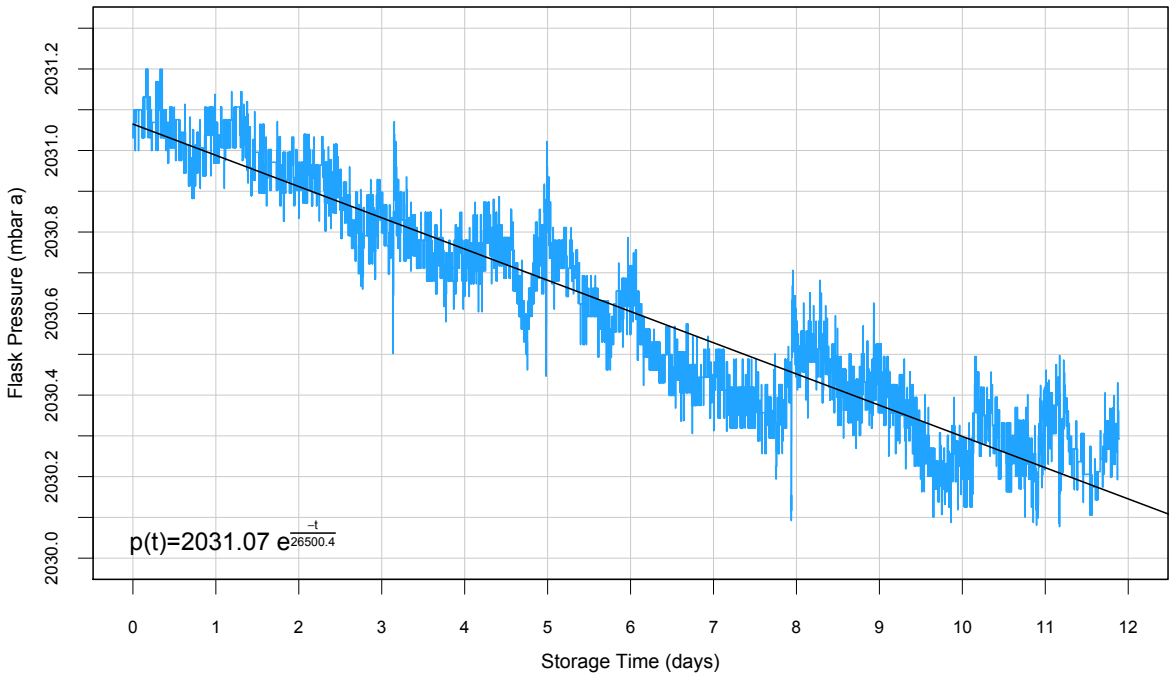

Figure 11 Temperature compensated pressure decay curve in a 0.7 L glass flask after a storage period of ~12 days. Initial pressure was 2031.07 mbar a and end pressure was 2030.29 mbar a. Values were fitted with a two-parameter model of exponential decay, which was obtained from a linear regression ($R^2 = 0.9087$) of the log-transformed measurement data.

Besides calculating the leak rate, it is also useful to know how long it would take until the internal flask pressure drops to a certain value caused by inadequate compression of the seal. Referring to this, the pressure decay in every pressurized system, which suffers from a sufficiently small leakage can be described as an exponentially decreasing function. This relationship is given by Equation 3.4.

$$p(t) = p_0 \cdot e^{-\frac{t}{\tau}} \qquad \left(\begin{array}{c} p(t_\infty) = p_{ambient} \\ p(t_0) = p_{flask} + p_{ambient} \end{array} \right) \tag{3.4}$$

The parameters of interest p_0 and τ can be obtained from a linear regression of the log-transformed data. Thus, Equation 3.4 becomes:

$$\ln p(t) = \ln p_0 - \frac{t}{\tau} \tag{3.5}$$

From Equation 3.5 it is obvious that the time constant τ and the initial flask pressure p_0 is represented by the reciprocal of the slope and the antilog of the intercept, respectively. With these estimated values the two-parameter model of exponential pressure decay can be written as:

$$p(t) = 2031.07 \text{mbar} \cdot e^{\left(-\frac{t}{26500.4 \text{ days}}\right)} \tag{3.6}$$

Presuming that the same amount of air is leaking through both flask valves, the duration for the decrease in initial flask pressure can be predicted according to Equation 3.7. To give an example, it takes 11.3 years until the internal flask pressure has reached 1500 mbar a, which reflects nearly the half of the over-pressure with which the flask was filled.

$$t = -\frac{\tau}{2} \cdot \ln \frac{p(t)}{p_0} \tag{3.7}$$

It has already been stated that PCTFE is characterized by a greater hardness compared to that of PTFE. That in turn requires a higher compressive load to force

the PCTFE seal onto the inner surface of the flask valve to achieve a proper squeeze. Hence, the compressive force, which is applied to the PCTFE seal depends substantially on the performance of the selected motor type in the PFP and its produced torque. In particular, the amount of torque which is delivered when the motor is accelerated after a valve plug reaches the narrow part of the valve when closed determines the amount of squeeze of the PCTFE-on-glass-seat and maintains the seal integrity. A simple indicator whether a proper squeeze of the PCTFE-on-glass seat can be achieved by an actuator is to examine the establishment of an adequate sealing line at the inner wall of a flask. Referring to this, Figure 12 shows a flask valve which was automatically closed by an actuator.

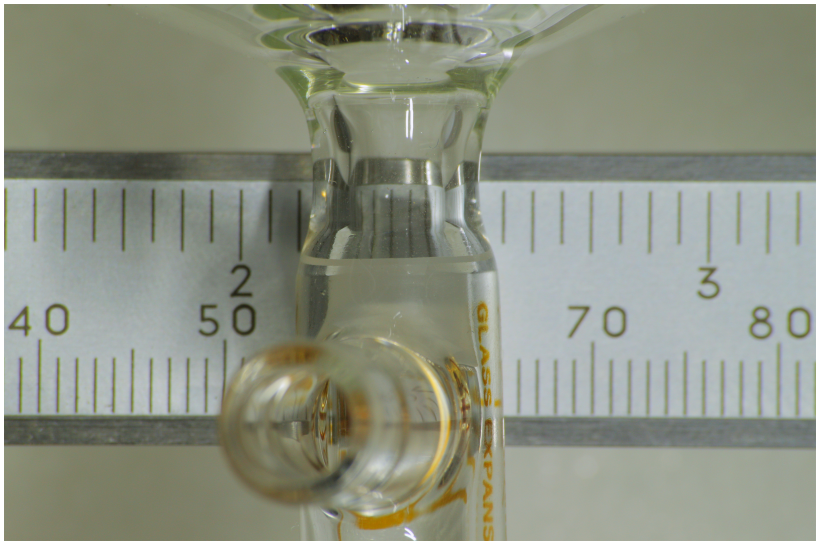

Figure 12 Sealing meniscus of a PCTFE-on-glass seat after a flask was closed by an actuator. The observed thickness of the sealing line (d ≈ 0.34 mm) is consistent with observations for other flask types equipped with the same glass stopper. (M. Rothe, personnel communication, November 10, 2009).

3.1.5 Conclusion

An approach was described to retrofit the flasks in the PFP with commercially available PCTFE-on-glass seats with minimal technical effort. This approach will reduce the influence of permeation and improve the sample quality if the PFP is exposed to long storage times. In order to examine if an adequate compression of the PCTFE seal can be achieved with the actuators, a leakage test was conducted using the pressure decay method. The pressure decay method is susceptible to distortion by external temperature variations and it is not possible to fully eliminate this influence by using Equation 3.2. With respect to this, the starting pressure p_0 was determined when the temperature remains constant for the first time which does not preclude that the temperature had completely stabilized in the flask.

Nevertheless, as the experimental results reveal, the leak rate is negligibly small, which is also confirmed by the large predicted amount of time until the inlet pressure decreases to the half of the initial filling pressure. However, the actual leak rate might be even smaller than the calculated, since possible additional sources of leakages in the whole test setup must be considered. This includes the needle valve, the two PTFE O-rings of the opened flask valve and all tube fittings, which were used to connect pressure transducer, needle valve and glass flask to the supply line. Moreover, the establishment of a distinct sealing line of contact after a flask valve was automatically closed is a further proof that the performance of the actuators do not affect the seal integrity of the harder PCTFE-on-glass seat.

3.2 Investigation of Memory Effects

3.2.1 Preliminary Consideration

The method of collecting air samples with overpressure consists of two fundamental steps. These are flushing and pressurizing and both together form the whole sampling procedure. As an indispensable presampling operation, the flushing process should remove any contamination from the flasks as well as from the sample transfer line in order to ensure that the air sample stream reaches the sample container in an unaltered state [10]. A sufficient flushing of the internal air sampling path is all the more important if flasks are connected in parallel, since long-residing artefacts at the inner surface of the sample tubing which are descending from previous sample air can adulterate the actual content of every subsequent flask sample. This so called memory effect can led to a sampling bias and contribute a significant source of error, in particular on sensitive measurements of carbon isotopes and oxygen.

Sample transfer lines for atmospheric air sampling applications are commonly constructed from smooth tubes made from stainless steel or from a composite of polyethylene/aluminium tubing with an ethylene copolymer coating on the inner side. Smooth tubes, by nature of their flat inner surface provide a maximum efficiency of flushing and are therefore the preferred kind of tubing in flask sampling devices. In contrast to this, essential components in the automated air sampling system, such as pumps, dryer and flasks are connected through corrugated tubes (321-4-X-6, Swagelok, Solon, USA), which are characterized by a semicircular tube profile. In general, due to there increased axial flexibility, the use of corrugated tubes can simplify the assembly of the internal sample air path. Regardless of this, in comparison with smooth tubes, corrugated tubes have

distinct disadvantages with respect to their flushing characteristics because of their convoluted tube profile. Depending on the geometry of the tube profile and the flow velocity of an incompressible fluid, which flows through a corrugated tube, different pattern of fluid flow in the convolutions can appear (see Fig. 13).

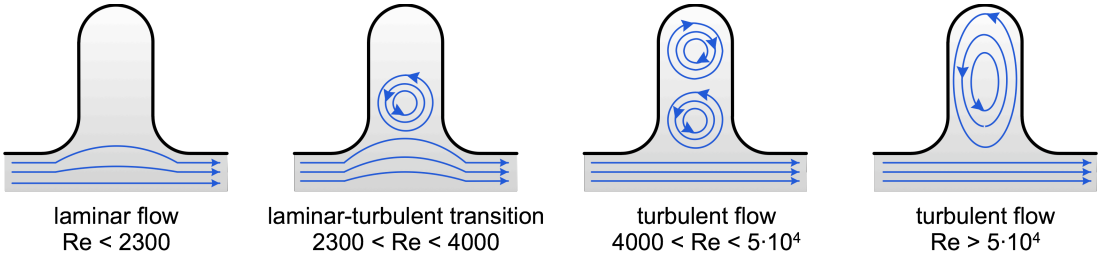

Figure 13 Flow of an incompressible fluid through a semicircular profiled tube. Depending on the flow velocity the establishment of turbulence within the convolutions can be observed. (Redrawn and modified from [61])

From Figure 13 it is obvious that a corrugated tube is only entirely flown through at high flow velocities ($Re > 5 \cdot 10^4$). This is primarily based on the development of a turbulence that fills the whole convolution. On the other hand, at Reynolds numbers $4000 < Re < 5 \cdot 10^4$ the development of two eddies can be observed. The primary eddy (below) lifts the secondary eddy (above) and restricts any significant mixture between convolution and core region of the tube. Furthermore, for regimes of laminar flow ($Re < 2300$) and laminar-turbulent transition ($2300 < Re < 4000$), main stream flow and turbulence does not extend into the whole convoluted tube profile, respectively [61].

To apply the above described effects to a gas flow, the gas has to be treated as incompressible and the change in volume can be neglected for practical applications. This consideration is acceptable as long as the gas flows with Mach numbers $Ma \leq 0.2$ [62]. Supposing that sample air passes through the corrugated tubing in the sampling system and that the system is operating with its maximum

flow rate of approximately 20 L min^{-1} the Mach number of the air sample stream amounts to 0.03 according to Equation 3.8. In Equation 3.8 is Q the volumetric flow rate, d the inner diameter of the corrugated tube and c the speed of sound (c = 343 m s^{-1} at T = 20°C [62]). Since 0.03 << 0.2, it is reasonable to assume that the motion of the sample gas flow is not essentially different from that of an incompressible fluid.

$$Ma = 4\frac{Q}{c\pi d^2} \tag{3.8}$$

At this point it is necessary to asses which kind of flow regimes can appear in the corrugated tubing when air is drawn through the flask sampling system. Table 3.2 provides values according to Equation 3.9 of Reynolds numbers together with typical flow rates at which the sampling system might be operated when deployed in the field or onboard aircraft.

$$Re = 4\frac{Q}{\nu\pi d} \tag{3.9}$$

Table 3.2 Reynolds numbers and flow regime for typical flow rates when operating the PCP/PFP. Calculations are based on the dimensions of the corrugated tube in the PCP/PFP; ν = 15 10^{-6} m^2 s^{-1} at T = 20 °C and p = 1013.25 mbar [62].

Flow rate L min^{-1}	**Reynolds number**	**Flow regime**
10	2228	*laminar flow*
15	3342	*laminar-turbulent transition*
20	4456	*turbulent flow (4000 < Re < 5 · 10⁴)*

These estimates suggest that the air flow in the corrugated tubing of the sampling system is affected by flow conditions at which a thorough flushing of the tube profile cannot be guaranteed (see Fig. 13). Taking this into account, the tubing might be an important source of systematic error that affects the integrity of the sample air that enters the sampling containers. For that reason, a laboratory test was carried out to investigate a possible memory effect associated with the corrugated tubing in the automated flask sampling system.

3.2.2 Laboratory Test

Before the experiment was conducted the flasks have been evacuated and conditoned similar to the flask pretreatment protocol of the MPI-BGC Central Flask Facility (see Appendix 1). The experiment involved air with different trace gas concentrations from two aluminium high-pressure gas cylinders (hereinafter referred to as tank A and B). Both tanks were filled with dry natural air using the air pumping facility at MPI-BGC. Furthermore, the predefined gas mixture of tank B was generated by spiking mole fractions of CO_2, CH_4, N_2O, SF_6, CO and H_2 with high concentration gases using the MPI-BGC gas blending unit (see Appendix 2). At MPI-BGC both air pumping facility and gas blending unit are used to generate precise gas mixtures to calibrate the in-situ instruments at the different monitoring stations of the MPI-BGC Tall Tower Network. Tank A (50 L) contained approximately the background atmospheric abundances of CO_2, CH_4, N_2O, SF_6, CO and H_2, whereas tank B (10 L) contained air far above ambient levels. The large difference in trace gas composition between tank A and tank B should ensure to obtain clear quantitative results, and that even small memory effects are still at a detectable level. Referring to this, the chosen target concentrations reflect nearly five times of their daily maxima that can usually be observed at numerous

continental atmospheric measurement stations in Europe (e.g. https://ramces.lsce.ipsl.fr/). The different mole fractions of the test air in both tanks are displayed in Table 3.3.

Table 3.3 Composition of air from the two high-pressure tanks that were used for the experiment.

Analyte	**Mixing ratio**			
	Tank A*		**Tank B****	
CO_2	387.59	ppm	2250	ppm
CH_4	1931.23	ppb	11000	ppb
N_2O	323.92	ppb	1650	ppb
SF_6	20.83	ppt	50	ppt
CO	141.35	ppb	1500	ppb
H_2	565.95	ppb	40000	ppb

* Tank was analyzed by the MPI-BGC GasLab.

** Gas mixing ratios were derived from calculations (see Appendix 2).

Both gas cylinders were equipped with two-stage stainless steel regulators (tank A with 5114D580 and tank B with 5114C160, Air Liquide, Plumsteadville, USA) and connected to a three-way valve (SS-43GXS4 ,Swagelok, Solon, USA) to switch between the two gas mixtures. In order to protect the test air stream derived from tank A from O-ring effects in the regulator, the air from tank A was pulled into the sampling line (1/4“ OD, Synflex, Saint-Gobain, Courbevoie, France) with a greater flow rate than achieved by the two-stage compressor in the PFP, whereby the remaining air was exhausted to atmosphere through a split tee (SS-2000-3, Swagelok, Solon, USA) installed in downstream direction. Furthermore, a second three-way valve (SS-43GXS4, Swagelok, Solon, USA) was used to continuously flush the sampling line of tank A when air was drawn from tank B to the PFP.

During the experiment both tanks were orientated horizontally in order to reduce gravimetric fractionation of CO_2 concentrations [63]. The whole experimental setup is illustrated in Figure 14.

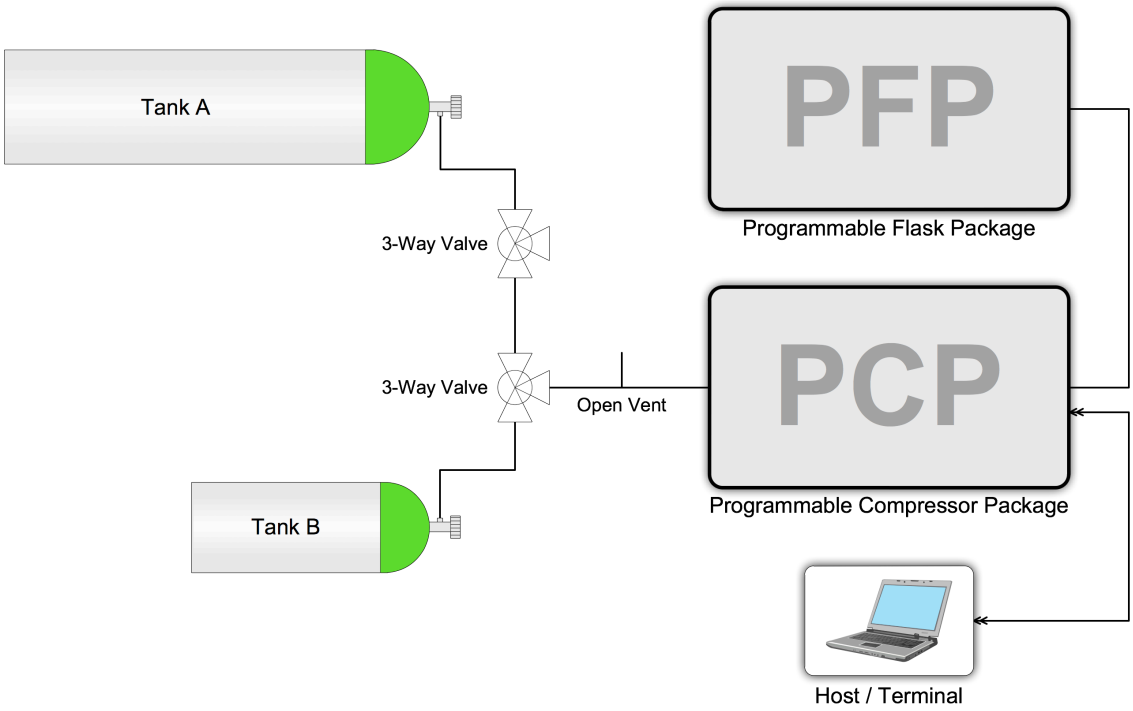

Figure 14 Experimental setup to investigate sample-tube induced memory effects: The flasks in the PFP were filled with air from two high-pressure gas cylinders containing different trace gas mixing ratios. A three-way valve was used to switch between the two gas mixtures. The sampler was operated in manual mode using a terminal emulator.

Before the flasks were filled, the whole sample air path was flushed for 5 min with air from tank A at a flow rate of approximately 20 L min^{-1}, which is consistent with the sample flow rate during the experiment. To visualize an eventual memory effect in the twelve flasks following sampling protocol was chosen as shown in Table. 3.4.

Table 3.4 Sampling protocol of the experiment to investigate a possible memory effect.

Flask	Sample air
1	tank A (close to atmospheric levels)
2	tank B (above ambient levels)
3 - 12	tank A (close to atmospheric levels)

All flasks were sampled in that order as they are connected to the sampling line. The first flask in the PFP was filled with the low-concentrated reference gas from tank A whereas the second flask was filled with the high-span gas supplied from tank B. Immediately after the second flask was filled, all subsequent flasks were sampled with air from tank A. With this procedure, it is expected to obtain a distinct pattern that shows: First, a mixing ratio for the first flask in the sampling line that is close or equal to the reference value of tank A, because this flask is not affected by artefacts from the high-span gas. Secondly, flasks which are installed behind the second flask will show higher mixing ratios than the first flask caused by residual air potentially remaining in the tubing of the sampler. Thirdly, the effect becomes weaker as a function of flask position (e.g. before the last flask in line gets filled, the tubing was flushed ten times with the reference gas from tank A).

During the filling procedure of the second flask, air from tank A was continuously exhausted through the first ball valve in the sampling line. All flasks were filled with an overpressure of 1 bar. With approximately one minute, the flushing time (30 s manifold flushing and 30 s flask flushing) was kept as short as possible. In order to obtain reproducible values, the whole sampling cycle (including flask conditioning and filling) was repeated three times. For flask analysis the sampling containers have been dismounted from the PFP.

3.2.3 Flask Analysis

The methods to analyse trace gas concentrations in flasks as well as in gas cylinders were carried out by the gas laboratory department (GasLab) of the MPI-BGC and have been in routine use since 1999 [64].

The centerpiece of the analytical setup is a modified gas chromatograph (GC) (WSHP6890NGC, Hewlett Packard, Palo Alto, USA) equipped with different detectors, two main chromatographic columns and two 10 port injection valves. The detectors used for trace gas detection and the average precisions that are achieved by the MPI-BGC GasLab are listed in Table 3.5.

In order to calculate reliable statistical parameters flasks have been at least analyzed two times for each specie. The second flask was not analyzed because the remarkably high trace gas concentrations with which the flask was filled exceeded the calibration scale of the MPI-BGC GasLab.

Table 3.5 Average precisions of trace gas mixing ratios achieved at the MPI-BGC GasLab and corresponding GC detectors (A. Jordan, personnel communication, April 12, 2010).

Analyte	**Analytical precision**	**Detector**
CO_2	0.07 ppm	*flame ionization detector (FID)*
CH_4	1.5 ppb	
N_2O	0.2 ppb	*electron capture detector (ECD)*
SF_6	0.05 ppt	
CO	1 ppb	*reduction gas detector (RGA)*
H_2	3 ppb	

3.2.4 Results

The results of the flask analysis are listed in Appendix 3. They contain the arithmetic mean of the repeated flask measurement, the standard deviation and the number of measurement repetition. The results have been averaged by weighting the arithmetic means of each trace gas mixing ratio according to their measurement repetitions and to the number of test cycles. The formulas for statistical analysis are given in Appendix 5 [65]. The results are illustrated in Figure 15.

First of all, it is important to note that for the gases N_2O, CO and H_2 the value of flask 9 differs clearly from the rest of the data points. In particular, it reflects the maximum for N_2O and CO and the minimum for H_2. Reason for these deviations might be the replacement of the original sampling container with a flask type from another manufacture (Normag GmbH, Ilmenau, Germany) that was used to accomplish the third sampling cycle. The replacement was necessary because of a valve breakage of the original flask. Although the replaced glass flask has been flushed over an extensive period (nearly 1 hour at 10 L min^{-1}) with air from tank A before used in the experiment, it was not subjected to an evacuation procedure, which is part of the flask pretreatment protocol (see Appendix 1). Thus, this flask value will be treated as an outlier and ignored for the following discussion.

As displayed in Figure 15, all analyzed species show enriched mixing ratios in flasks that were filled after the high-span gas has passed the sampling system. Nevertheless, with exception of CO_2, all flask values lie within the range of the average precisions (drawn as error bars) achieved by the MPI-BGC GasLab (see Table 3.5). This is indicated by an overlap of the error bars and implies visually that there is no significant differences between the weighted means of the flask (1) filled with background air from tank A and flasks (3-12) that have been sampled

shortly after the second flasks was filled. However, the CO_2 results show a memory effect. Furthermore, flask three shows a higher mixing ratio (387.77 ppm) than the background value (387.61 ppm), which cannot be attributed to uncertainties in analysis precision.

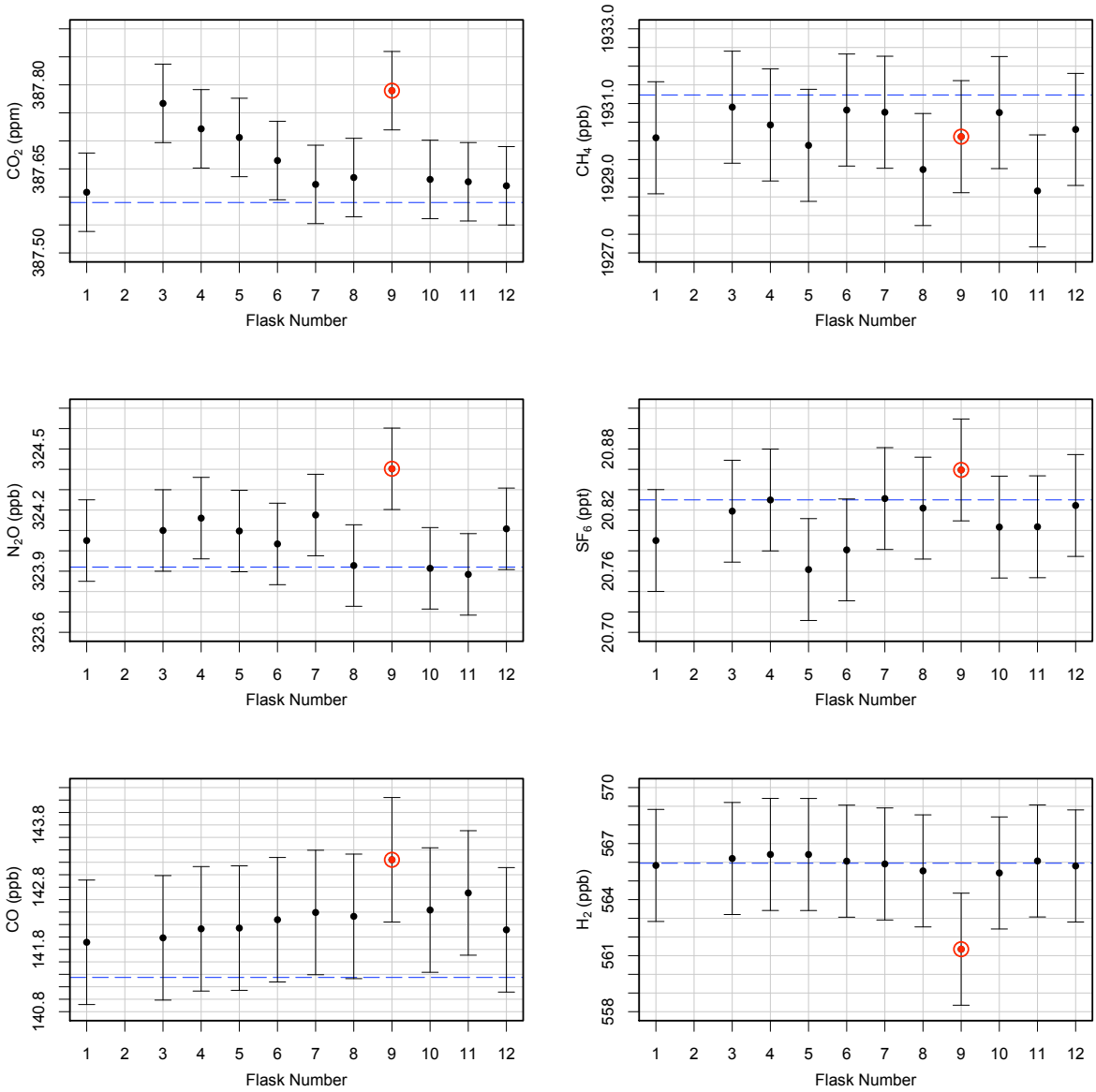

Figure 15 Trace gas concentrations (CO_2, CH_4, N_2O, SF_6, CO, H_2) in the flask samples: Values present the weighted mean according to the number of test cycles and measurement repetitions. The blue dotted line shows the corresponding mixing ratio from tank A. Error bars indicate the average precision of the MPI-BGC GasLab. Flask 9 (red) can be considered as an outlier. Due to valve breakage the flask was exchanged with a similar type from Normag GmbH.

To quantify how much residuals of the high-span gas are contained in the flasks, variations within the CO_2 flask series can be expressed as a relative value. This relationship is given by Equation 3.10.

$$\varepsilon = \frac{x_{[CO_2, \text{Flask i}]} - x_{[CO_2, \text{Flask 1}]}}{x_{[CO_2, \text{Flask 2}]} - x_{[CO_2, \text{Flask 1}]}} \tag{3.10}$$

Presuming that the CO_2 mixing ratio in the second flask is equal to that in tank B Equation 3.10 can be simplified to:

$$\varepsilon = \frac{\Delta x_{CO_2}}{1862.5 \text{ ppm}} \tag{3.11}$$

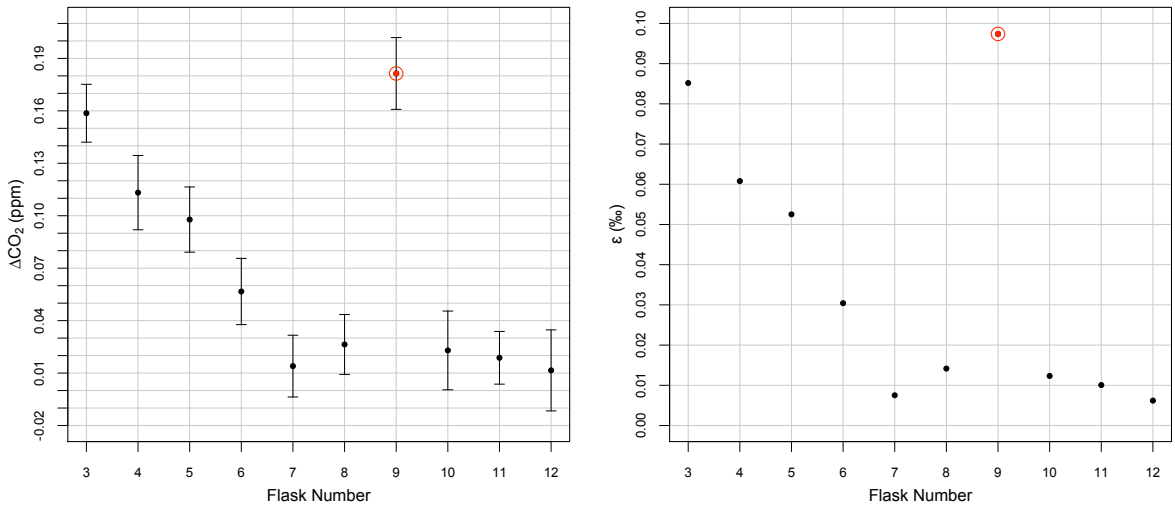

Figure 16 Variations within the CO_2 flask series expressed as absolute and relative values. Left graph shows the difference between flask 1 and flasks the were sampled after the high-pan gas has passed the sampling system. Right graph shows values according to Equation 3.11. Flask 9 (red) is supposed to be an outlier. Error bars indicate the standard error and were calculated assuming that flask values are statistically independent (see Appendix A 5).

Figure 16 shows that the mixing ratio in flask three is about 0.16 ppm higher compared to the background value in the first flask. Presuming that the enrichment is induced through artefacts of the high-span gas this is equal with 0.085‰ residual air from the previous flask filling. For the rest of the flasks (4-12) ε is close to or smaller than 0.06‰. However, the corresponding mixing ratios are still within the average precisions of the MPI-BGC GasLab as illustrated in Figure 15.

3.2.5 Conclusion

An experiment was performed to evaluate a possible memory effect associated with the imperfect flushing characteristics of the corrugated tubing inside the sampler. As the results of the flask analysis demonstrate, there is no discernible trend indicating that artefacts from a previous flask sampling procedure have a significant bias to subsequently filled flasks. Although the results for CO_2 might suggest a memory effect, associated changes in CO_2 mole fraction are substantially small and can be neglected. Furthermore, fluctuations of atmospheric trace gas concentrations under real field conditions appear in magnitudes much smaller than they were simulated in the experiment. Increasing the flushing time up to several minutes when the system is deployed in the field will also ensure that artefacts from previous filling activities are efficiently removed from the sampling tubing.

3.3 Assessing the Suitability to Validate Continuous Measurements

3.3.1 Preliminary Consideration

Flask samples are also called instantaneous or grab samples, since they are collected instantaneously, usually within minutes or even less. Hence, a flask sample only reflects the atmospheric conditions at the sampling site for a short period of time. For that reason, flasks must be collected at times when concentrations are expected to be representative of the typical site conditions both spatially and temporally [66]. In general, flask samples are very sensitive to short-term fluctuations and therefore different factors have to be taken into consideration when deciding to fill a flask in order to meet the aforementioned requirements on the moment of sampling [67]. Furthermore, a single flask sample is not the best estimate of the daily mean concentration because it cannot reflect the whole diurnal cycle of CO_2 (1). Thus, in contrast to continuous measurement systems flask samples are only partly suitable to study local long-term variations of atmospheric trace gas concentrations. However, it is a common practice to complement continuous in-situ measurements of GHGs performed at ground-based stations with an additional flask sampling program, because data derived from flask samples can be useful to replace the continuous data if not available (e.g. maintenance, malfunction). Furthermore, flask samples can serve as an additional verification on the accuracy of the continuous measurement system [e.g. 14, 68]. Conversely, the continuous measurement record can help to confirm for instance enriched flask values as a result of real short-term fluctuations, which would be otherwise considered as outliers and removed from the data set [67]. In

this way, flask data can be used to validate continuous measurements and vice versa.

In order to asses the suitability of flask samples collected with PCP/PFP to validate a continuous measurement system, the sampler was operated in combination with a state of the art greenhouse gas analyzer. With regard to the current state of the evaluation process of the instruments to be integrated into the ICOS AS, this analyzer was chosen to provide the continuous on-site CO_2 and CH_4 measurements for the future ICOS Atmospheric Observation Network.

3.3.2 The Cavity Ring-Down Analyzer

The most popular techniques of measuring concentrations of GHGs are the non-dispersive infrared spectroscopy (NDIR) for CO_2 and gas chromatographs (GC) for CH_4 and both are widespread in use at the majority of observatories in the different air sampling networks [e.g. 69, 70]. Nevertheless, these measurements are performed on extremely dried sample gas streams (e.g. dew point = -80 °C [69]) and require frequent and costly calibrations to avoid any long-term drift.

Recently, the cavity ring-down spectroscopy (CRDS) has been established as an alternative method for making measurements of CO_2 and CH_4 in the atmosphere. This approach permits a measurement of the adsorption directly in the humid sample gas stream and circumvents the above mentioned limitations of NDIR and GC [71]. Since its introduction at the MPI-BGC in 2009, the CRDS technique has been proven as a reliable tool to acquire high-accuracy continuous measurements of atmospheric levels of CO_2 and CH_4 during aircraft and tall tower observations [68, 72].

Ring-down spectroscopy is based on the principle of measuring the rate of decay of light inside an optical measurement cell. Operationally, mono-chromatic radiation from a pulsed laser is injected into a stable optical cavity defined by two or more high-reflectivity mirrors. After cavity and laser have come into resonance, the light is transmitted out of the cavity and monitored using a photodetector (e.g. photodiode). Once the detector registers a signal above a certain threshold, the laser beam is abruptly interrupted and the light intensity is measured as it decays in the cavity (see Fig. 17) [73].

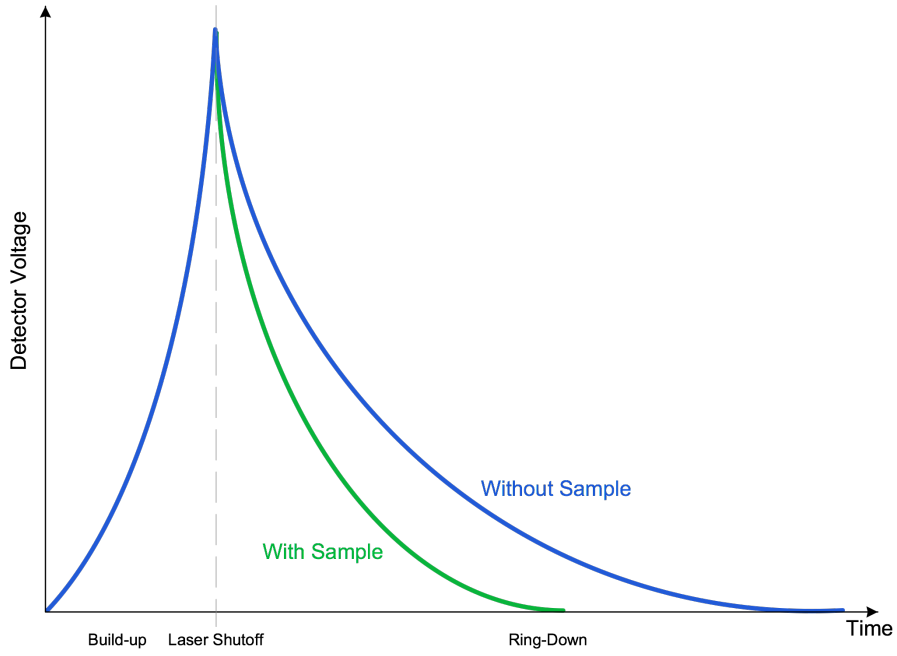

Figure 17 The detector signal which is proportional to the light intensity, as a function of time in a CRDS system without and with a sample having resonant absorbance. After the laser is turned off the ring down time for the light to decay is slower if the cavity is empty compared to the cavity containing molecules that absorb at the laser wavelength. (Redrawn from [74])

The intensity $I(t,\lambda)$ of the transmitted light from the cavity decays exponentially in time and can be written in a form analogous to the Lambert-Beer formula for absorption (see Eq. 3.12) [73].

$$I(t,\lambda) = I_0 e^{\left[\frac{-t}{\tau(\lambda)}\right]} \tag{3.12}$$

For an empty cavity, the decay time constant τ_0 is only determined by the reflectivity of the mirrors R(λ) according to Equation 3.13 [75].

$$\tau_0(\lambda) = \frac{d}{c|\ln R(\lambda)|} \tag{3.13}$$

Provided that a sample gas is introduced in the cavity, the absorption of the sample can be obtained by taking the difference between the ring-down time $\tau_0(\lambda)$ of the empty cavity and the ring-down time $\tau(\lambda)$ of the cavity containing the sample. This relationship is given by Equation 3.14 [75].

$$\alpha(\lambda) = \frac{1}{c}\left[\frac{1}{\tau} - \frac{1}{\tau_0}\right] \tag{3.14}$$

The CRDS analyzer (G1301, Picarro, Sunyyvale, USA) used for the experiment was developed by Picarro Inc. and is capable to measure simultaneously atmospheric levels of CO_2, CH_4 and water vapor. The main components of this cavity ring-down spectrometer are two tuneable diode lasers (TDL), a high-finesse optical cavity formed by three high-reflectivity mirrors (R(λ) > 99.995%) and a photo-detector. The TDLs are tuned to emit light at a wavelength of 1603 nm for measuring CO_2 and at 1651 nm to scan over the individual spectral lines of CH_4 and H_2O. Concentration measurements are provided every five seconds and the temperature as well as the pressure in the cavity are kept to be constant at 45 °C and 0.13 mbar, respectively, in order to maintain the stability of the two individual

spectral lines [76]. The block diagram of the basic components is illustrated in Figure 18.

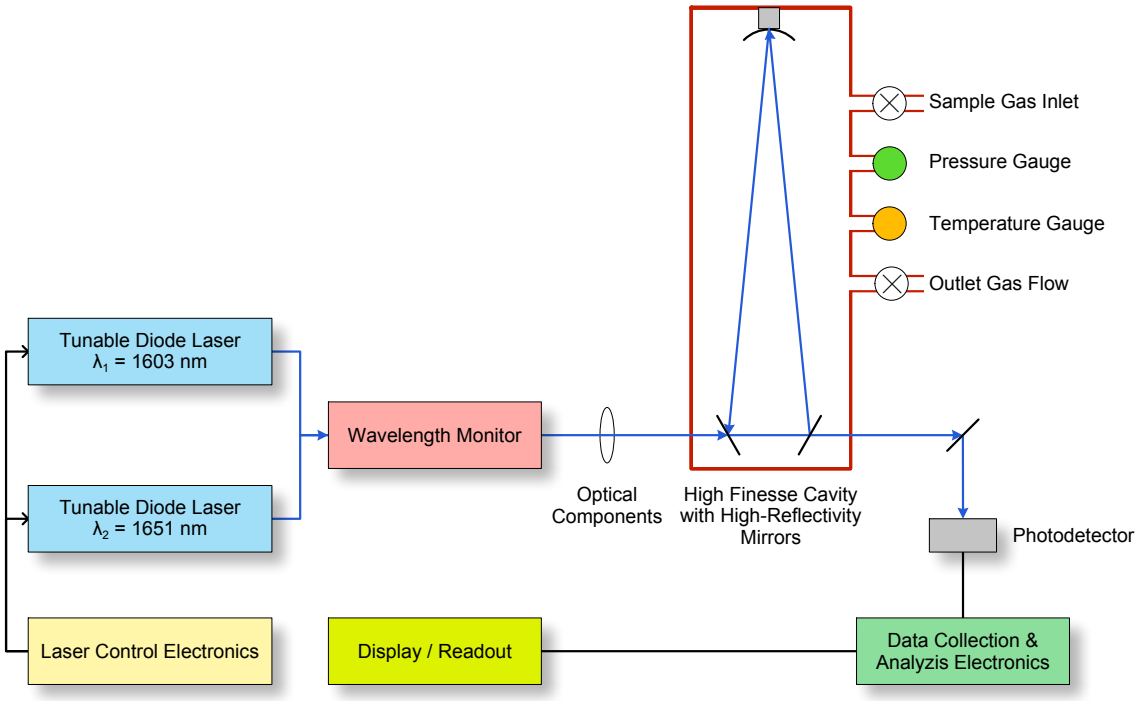

Figure 18 Block diagram of the CRDS analyzer. (Redrawn and modified from [76])

3.3.3 Laboratory Test

Before the experiment was conducted all flasks have been subjected to the pretreatment as described in Appendix 1. The air sample dryer was removed because for further investigations. The gap in the sample air flow path was bridged with polyethylene/aluminium tubing (1/4“ OD, Synflex, Saint-Gobain, Courbevoie, France)

Twelve flask samples were collected on a basis of 30 min in parallel to the routine in-situ measurements of the CRDS instrument. Sample air was drawn from the outside of the laboratory over the daytime period of 10:00 am to 16:00 pm. The sample air intakes of both instruments were placed close together (PCP/PFP: 1.5 m length, 1/4“ OD, Synflex, Saint-Gobain, Courbevoie, France; CRDS

Analyzer: 6 m length, 1/16“ OD, SS-T1-S-014-20E, Swagelok, Leipzig, Germany). The air stream supplied to the flask sampling system was effectively dried after passing through a drying column densely packed with magnesium perchlorate ($Mg(ClO_4)_2$; 02401119, PerkinElmer, Rodgau, Germany). This led to a decrease in the sample flow rate to approximately 9 L min^{-1}. The flushing time was set to 10 min (5 min manifold flushing and 5 min flask flushing) which is similar to the protocol for manual flask sampling at the MPI-BGC flask sampling network. All flasks have been pressurized to ~1 bar overpressure and were analyzed at the MPI-BGC GasLab (see Section 3.2.3). The whole experimental setup is illustrated in Figure 19.

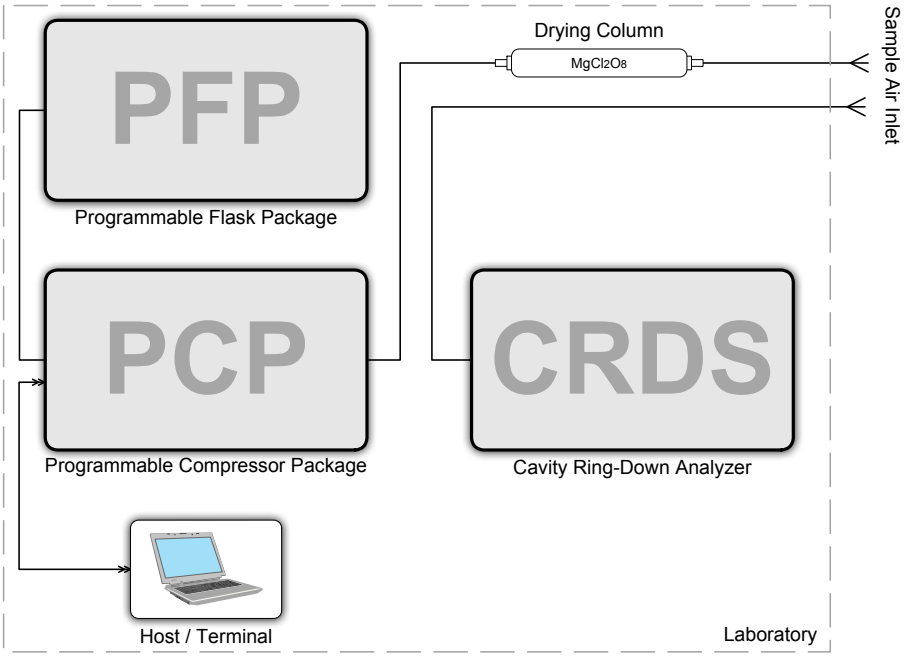

Figure 19 Setup of the intercomparison experiment carried out with the automated flask sampling system and a CRDS analyzer. Air was drawn from the outside of the laboratory. The sampler was operated in manual mode and flasks were filled every 30 min. The sample air stream which was supplied to the PCP/PFP was dried with anhydrous $Mg(ClO_4)_2$.

3.3.4 Results

The analysis results of the flask measurements are listed in Appendix 4. The raw in-situ data was prepared as follows: A correction function was applied to each record of the two species (CO_2, CH_4) in order to compensate the influence of varying water vapor concentration during the measurement period (see Eq. 3.15 and 3.16). Two major effects are associated with the presence of water vapor whicht have a direct influence on the mixing ratios of CO_2 and CH_4 and on the performance of the CRDS analyzer. These are the dilution of CO_2 and CH_4 as well as pressure broadening of their individual spectral lines [71, 72]. The water correction functions were derived from an experiment performed at the MPI-BGC in April 2010 (J. Winderlich, personnel communication, May 26, 2010).

$$x(CO_2)_{dry} = \frac{x(CO_2)_{wet}}{1 - 0.0119995 \cdot x(H_2O)_{CRDS} - 0.0002674 \cdot x(H_2O)^2_{CRDS}} \tag{3.15}$$

$$x(CH_4)_{dry} = \frac{x(CH_4)_{wet}}{1 - 0.0098232 \cdot x(H_2O)_{CRDS} - 0.0002393 \cdot x(H_2O)^2_{CRDS}} \tag{3.16}$$

In the end, the actual values for both gases were calculated by applying a calibration function to the water corrected data set (see Eq. 3.17 and 3.18; J. Winderlich, personnel communication, May 26, 2010).

$$x(CO_2)_{cal} = 1.003078109 \cdot x(CO_2)_{corr} - 0.727596214 \tag{3.17}$$

$$x(CH_4)_{cal} = 1.00671341 \cdot x(CH_4)_{corr} - 1.408226581 \tag{3.18}$$

In order to correlate the single flask values with the continuous record, the flask data was merged with the in-situ data. For that, a 10-second average of the in-situ

data was calculated which considers the flask filling time under experimental conditions, and that a small amount of air from the flushing process is still contained in the sampling container when pressurizing is completed. The sample period (5 s) was derived from the continuously logged manifold pressure (data output 1 s) during sampling and the History File of the PCP/PFP. The time interval being representative for the influence of the flushing procedure was assumed as 5 s.

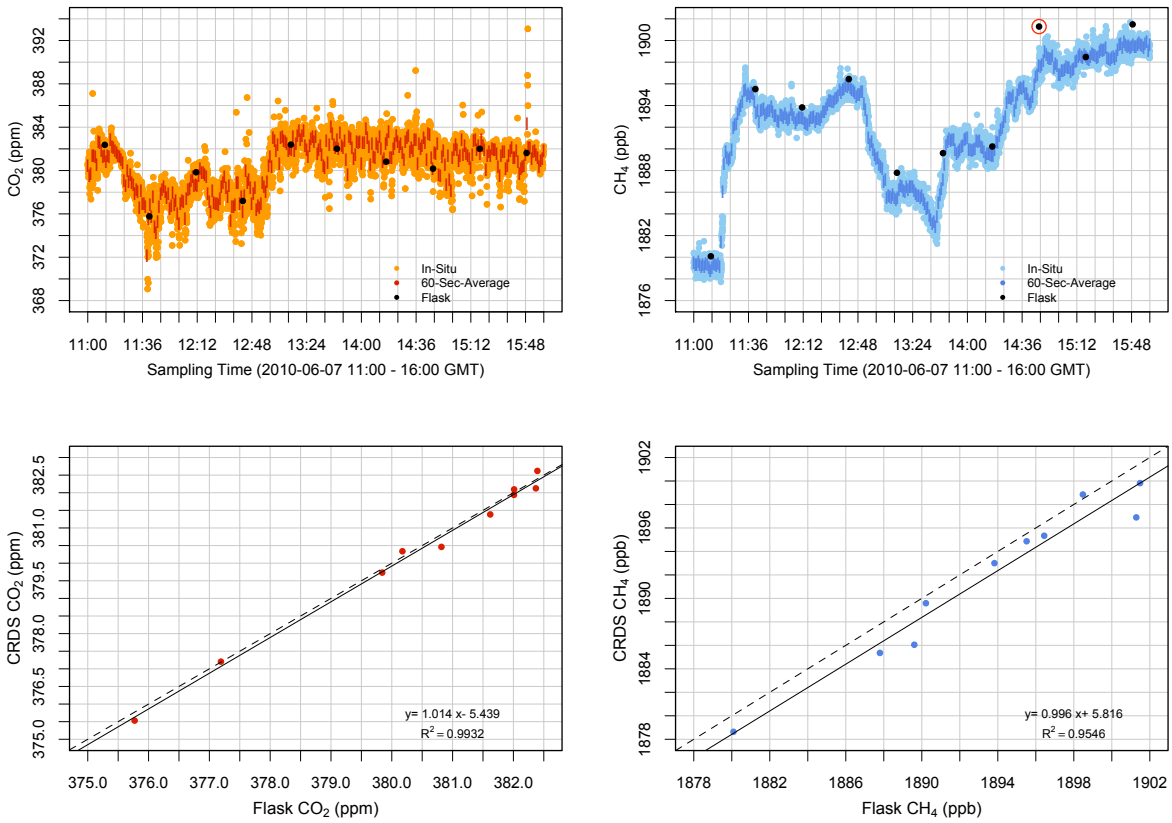

Figure 20 Intercomparison between CRDS measurements and flask values for CO_2 (left, red) and CH_4 (right, blue). Upper row: Time-series plot of the continuous data with an added 60-second average and the flask results (black dots). Bottom row: Scatter plot, with the dashed line denoting the one-to-one ratio. The black line represents the linear fit. Correlation coefficients (R^2) for both species are greater than 0.95.

In Figure 20 the red pattern corresponds to the CO_2 measurements obtained by the online system with a concentration ranging between 369 and 393 ppm and a half-hourly variability < 1.8 ppm. The black dots represent the flask measurements which are in good agreement with the CO_2 data. The strongest short-term variations (11:00-13:00 GMT), which are more clearly pronounced by the in-situ data, are captured by the flask values as well. The linear least-squares fit in the corresponding scatter plot reveals that CO_2 concentrations reported by both methods are highly correlated (R^2=0.99). Furthermore, the slopes of the regression line (1.014) and the one-to-one ratio (shown as dashed line) are close to unity.

The blue pattern in Figure 20 represents the real time CH_4 measurements. The concentrations range between 1877 and 1901 ppb with a half-hourly variability < 5.4 ppb. Although there is a reasonable agreement between online measurements and flask results (black dots), nearly all flasks reveal enriched concentration values. Particularly the sample taken at 14:47 GMT (marked by the red circle) shows a remarkably higher CH_4 mixing ratio than documented by the in-situ data. Nevertheless, variations in CH_4 mixing ratios are also reproduced by the flask series (e.g. 11:00-11:40 GMT) and a highly parallel relationship between both methods is shown by the R^2 value of 0.95 as well as a slope close to one (0.996). However, the distinct off-set between unity slope and linear fit suggests that the CH_4 measurements are possible biased.

For a further in-depth intercomparison, Figure 21 shows the absolute difference between discretized in-situ values and flask data as a function of the range of the time interval (10 s), which was applied to correlate both methods, to provide an indication of variability in the ambient air signal during the individual flask fillings. The greatest atmospheric variability in the discretized values (~3 ppm) in the CO_2 data corresponds to an absolute difference of -0.24 ppm. On the other hand, an almost identical value corresponds to the lowest atmospheric variability

(~0.09 ppm). Similar can be found for the CH_4 data: For a spread within the 10-second average of nearly 0.45 ppb, different ΔCH_4 values (-3.5 ppb & 0.37 ppb) can be observed.

This lead to the conclusion that uncertainties between both methods cannot be addressed to short-term variations of CO_2 and CH_4 during sampling, and are thus a result of a systematic bias which could arise either from the subsequent laboratory analysis (e.g. calibration error) or from the performance of the CRDS analyzer. The latter might be affected by a drift in the continuous measurements because the calibration of the CRDS analyzer took place several weeks before the experiment was conducted. In regard to tall tower applications, the instrument is usually calibrated at least every 100 hours [68].

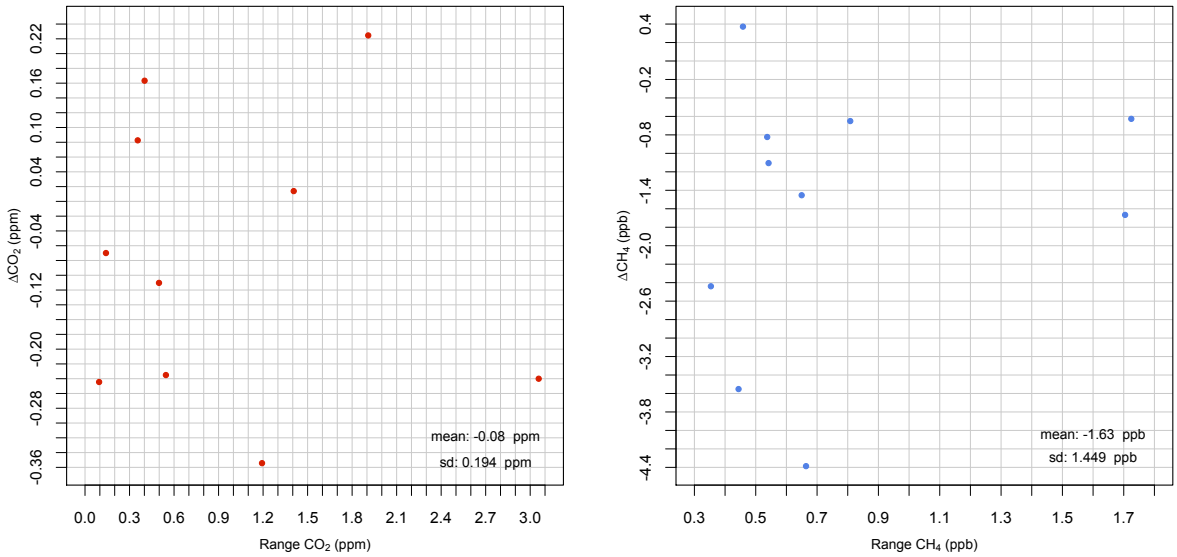

Figure 21 Intercomparison between CRDS measurements and flask values with regard to the atmospheric variability of CO_2 (left, red) and CH_4 (right, blue) during sampling. Absolute difference between discretized in-situ and flask values as a function of the range of the time interval (10 s) which was applied to the in-situ data.

3.3.5 Conclusion

An intercomparison experiment was carried out to assess the suitability of flask samples obtained by the PFP/PCP to validate CO_2/CH_4 measurements based on the CRDS technique. Although the CH_4 flask series shows slightly enriched values, the mean difference between in-situ and flask data for both CO_2 (-0.08 ppm) and CH_4 (-1.6 ppb) is small. Furthermore, the coherency in the time-series observation between the two measurements is obvious and all flask samples were able to capture the atmospheric variations of CO_2 and CH_4. Additionally, correlation coefficients greater than 0.95 confirm the representativeness of the flask samples.

However, in its basic configuration the automated air sampling system is only capable to capture atmospheric events within few seconds. The main cause for this is the high sample flow rate (20 L min^{-1} typical at sea-level) created by the two-stage compressor, which is dimensioned for aircraft-borne platforms where sampling takes place under conditions of low ambient pressures. Nevertheless, what is an important technical aspect for deploying the PCP/PFP onboard aircraft, is a clear disadvantage for ground-based sampling. Recently, a tall tower design was presented using stainless steel spheres that act as buffer volumes on the sample lines [68]. It is envisioned to integrate that approach into the design of the ICOS AS as well since the buffer volumes provide a physical integration of atmospheric variability over more than 30 min. This allows for almost simultaneous measurements from the different measurement heights of the tall tower carried out with only one CRDS analyzer. If flask data has still to be comparable, the sampling time needs to be extended. This can only be achieved through a reduction of the sample flow rate. Additionally, a lower flow rate would also reduce the scatter of the flask measurements on the time-series since variations in the ambient air signal will be covered over a more extended period.

Chapter 4

Final Conclusions and Outlook

This diploma thesis has addressed the initial evaluation of an automated air sampling system, originally designed for aircraft sampling, to assess the feasibility for using the system in a network of continental monitoring stations within the European ICOS infrastructure project. The automated air sampling system is described and initial results are presented in order to draw conclusions about steps that need to be taken in the ongoing development process for the system to operate at a surface station.

4.1 Improvements and Laboratory Tests

Two experiments have been carried out to verify the instrument performance, and both of them - the investigation of potential memory effects and the intercomparison experiment - showed that it is possible to obtain representative flask samples of important greenhouse gas species with the sampler in its current configuration. The results of the intercomparison experiment have revealed that a reduction of the sample flow rate will be necessary to ensure the comparability between flask data and continuous measurements which are carried out by using the integrating effect of air buffer volumes. This will require further tests under operating conditions representative of the planned ICOS AS air inlet design.

Nevertheless, a lowesr sample flow rate also implies that the occurrence of a sample-tube induced memory effect can become more significant than reported in section 3.2. It is therefore reasonable to replace the entire corrugated tubing with smooth stainless steel tubes. This will generally improve the quality of the flushing procedure and reduce the risk of accumulation of artefacts of water inside the tubing as a result of the recovery mechanism of the dryer, since the trapped water is evaporated through the sampling tube (see also Sect. 2.3.3).

Furthermore, a technical approach was found to retrofit the flask valves with commercially available PCTFE-on-glass-seats in order to reduce the influence of permeation. With this approach, a consistent sample quality during flask storage and transport can now be maintained. This is particularly crucial for sensitive measurements of O_2/N_2 and isotopic ratios. The associated leak test indicated full compatibility with the sampling containers and that the seal integrity is not limited by the performance of the actuators. The latter finding has implications for further system modifications concerning the flask package. Among others, it is planned to accommodate the PFP to larger flask volumes since the current sample volume is not sufficient for analysing the whole set of ICOS core parameters in one single flask. Especially, integrated $^{14}CO_2$ sampling and analysis require a large portion of sample air (up to 2.5 L) which cannot be achieved with a flask volume of 0.7 L [11]. The new flask types will be designed and manufactured by Normag GmbH and are standardly equipped with PCTFE-on-glass seats. It is therefore important to know at an early stage of the evaluation process that the actuators will be operational with harder PCTFE seals.

In general, flask samples in the experiments were acquired manually and their analysis was limited to CO_2, CH_4, N_2O, SF_6, CO and H_2. Further investigations which are focused on the representativeness of the sampling procedure must also include measurements of O_2/N_2 and isotopic ratios of CO_2, and it will be

indispensable to prove the reliability of the instrument under field conditions. To that end, flask sampling should be triggered fully automatically in a continuous diurnal as well as in a periodic sampling mode.

4.2 Ongoing Work and Outlook

As already stated in section 2.3.3, the thermoelectrical dryer was not fully developed and operational when the work on this thesis began. Therefore, additional tests and investigations with the air drying system have been performed. These experiments are not included in chapter 3 since the further development of this unit could not be completed in the course of this diploma thesis. Nevertheless, the technical approach is described to bring the air sample drying system into operation and to improve the cooling performance.

Tests with the TEC and the corresponding controller board revealed that the circuit of the Peltier modules (SH10.125.05.L1.RTW.W18, Laird Technologies, Chesterfield, USA) generates an operating current higher than that of the power transistors (FDS3672, Fairchild, South Portland, USA) which are responsible for controlling the cooling capacities of the TEC. For that reason, all existing transistors have been replaced with more appropriate models (TPCA8004-H, Toshiba, Ismaning, Germany) that are capable to operate at a higher current. Furthermore, Peltier modules (PC-128-10-05, Supercool, Gothenburg, Sweden) with a greater cooling performance and better thermal cycling properties were selected. In conjunction with this, essential components of the TEC such as heat sinks and drying trap have been modified to meet the specific requirements of this technical approach. Comprehensive tests are yet to be carried out to assess whether the final design will guarantee a safe and efficient drying process. Two key questions remain: First, what dewpoint can be reached for a flow of

atmospheric air moisturized to 100% relative humidity? Second, what is the moisture capacity of the water trap and the associated recovery cycle to make continuous operation possible?

The air drying unit is just one of several improvements and modifications that are required to get from the current status to a final prototype that can be successfully integrated into the ICOS Atmospheric Station. Main tasks for the ongoing evaluation phase will be:

- Development of an mechanical interface to separate the actuator assembly from the flask unit assembly with the aim of enhancing the usability during flask replacement and reducing logistical costs.

- Redesign of the flask unit assembly to equip the PFP with larger glass flasks (this task is closely linked with the development of the mechanical interface concept).

- Development of a communication software to control the air sampling system with a central computer through the RS-232 serial interface.

- Implementation and development of an interface concept to integrate the flask unit into the infrastructure of the Central Analytical Laboratory for providing automated analysis without removing the sampling containers.

In the final design, the automated air sampling system will offer greater flexibility and usability to operate in a stationary, unattended, and low-maintenance scenario. This will make the instrument a vital component in future observational studies in global carbon cycle research within the ICOS research infrastructure and will make it possible to run the ICOS Atmospheric Network in optimal fashion.

Appendices

Appendix 1: Flask Pretreatment

An important part of every flask sampling strategy is to subject the flasks which will be later filled in the field to an appropriate pretreatment. The pretreatment usually comprises of evacuation and conditioning. An initial evacuation is necessary to clean the flasks from contaminations and particular matter of moisture stemming from the manufacturing process or previous sampling activities. In the second step, flasks will be flushed and filled with dry air that resembles the expected air in its analyzed constituents at the sampling site. This procedure should avoid the loss of analytes due to adsorption effects at the inner glass surface of the flasks after they have been filled in the field [58].

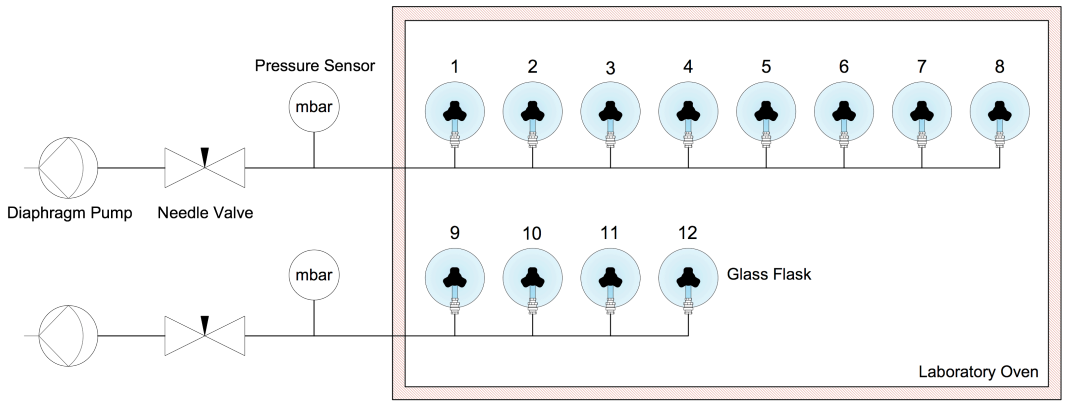

Figure A1 Principle of the evacuation unit: Flasks were evacuated for 72 hours at 60°C.

The sampling containers have been evacuated for 72 hours using two vacuum diaphragm pumps (N813.4ANE, KNF Neuberger, Freiburg, Germany) by keeping

them at 60 °C in a laboratory oven (UME700, Memmert, Schwabach, Germany) as illustrated in Figure A1. The air flow path was opened and closed with a needle valve (SS-BK, Swagelok, Solon, USA). During the evacuation procedure the system pressure was continuously monitored with absolute pressure transducers (VSP 521, Thyracont, Passau, Germany).

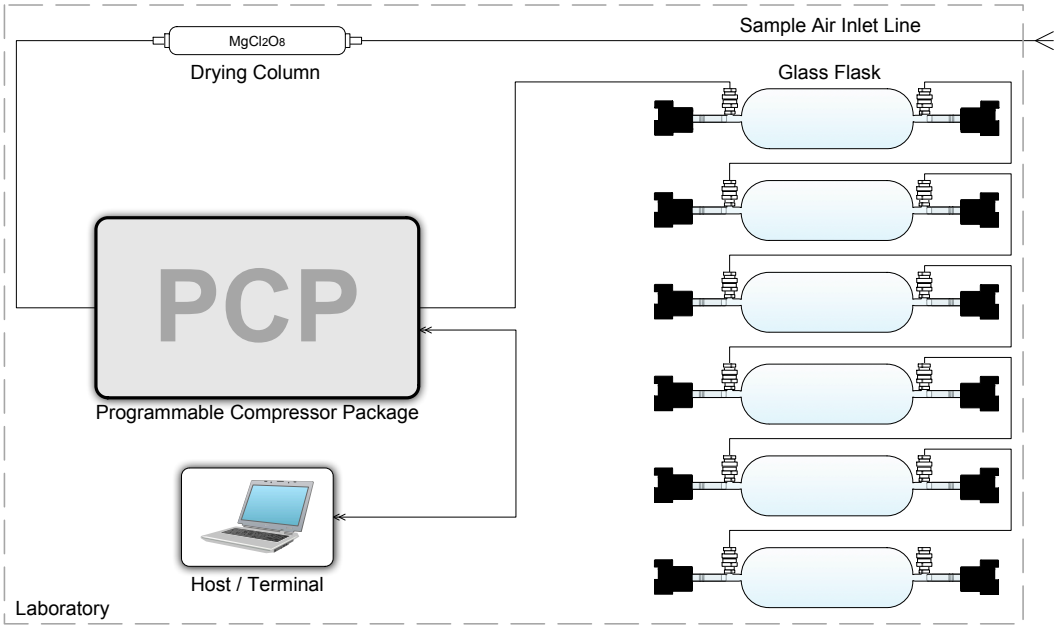

Figure A2 Setup for conditioning the 0.7 L flasks. Six flasks were connected in a row to the PCP. Flasks were flushed over a period of one hour with a flow of 10 L min^{-1} of air sucked from the outside of the laboratory. Air was dried with $Mg(ClO_4)_2$.

Flask conditioning was performed by connecting six flasks in a row with vacuum fittings (SS-4-UT-6-400 & SS-6-UT-1-4, Swagelok, Solon, USA) to the PCP (see Fig. A2). In that way, all flasks were flushed over a period of one hour with a flow of 10 L min^{-1} of mid-afternoon atmospheric air sucked from the outside of the laboratory. The air was dried using a drying cartridge filled with anhydrous magnesium perchlorate.

Appendix 2: Preparation of Reference Air Mixtures

Reference air mixtures at MPI-BGC are prepared in high pressure aluminium cylinders to calibrate continuous operating measurement systems at different sites within MPI-BGC Tall Tower Network and to supply other participating research groups. Cylinders are filled with natural air sucked from the outside of the laboratory of the MPI-BGC using an oil free compressor. The air is dried by passing several cartridges filled with anhydrous magnesium perchlorate ($Mg(ClO_4)_2$). Furthermore, the air is filtered with mole sieves to trap SF_6, N_2O and CO_2. After a cylinder is filled it gets analyzed by the MPI-BGC GasLab.

For increased standards above ambient levels several cylinders with very high mole fractions of CO_2, CH_4, N_2O, SF_6, CO and H_2 are used. The desired amount of the trace gas is put into a transfer volume higher than ambient pressure and pushed with a carrier gas (low concentrated natural air) into the cylinder. The pressure at which the transfer volume needs to be filled to spike a cylinder is calculated according to following Equation.

$$p_{Target} = \left(x_{Target} - x_{Ambient}\right) \cdot \frac{V_{Tank} \cdot p_{Tank}}{V_{Transfer} \cdot x_{Spiking}}$$

p_{Target} = target pressure of the spiking gas in the transfer volume

p_{Tank} = cylinder filling pressure

$x_{Target} / x_{Ambient}$ = target mole fraction / ambient mole fraction

$x_{Spiking}$ = mole fraction of the spiking gas

$V_{Tank} / V_{Transfer}$ = cylinder volume / transfer volume

Appendix 3: Flask Analysis Results of the Memory Effect Experiment

Note: Mean values are rounded to two significant numbers.
Standard deviations are rounded to three significant numbers.
Flasks from a sampling cycles indicated with * have not been analyzed due to valve breakage.

Flask Analysis Results: CO_2

Flask No.	Sampling cycle	$\bar{x}$ (ppm)	s (ppm)	n
1	1	387.59	0.063	4
	2	387.60	0.041	2
	3	387.63	0.056	4
3	1	387.7	0.031	3
	2	387.57	0.001	2
	3	387.88	0.058	5
4	1	387.62	0.105	3
	2	387.56	0.101	3
	3	387.88	0.043	5
5	1	387.64	0.106	3
	2	387.62	0.006	2
	3	387.78	0.029	5
6	1	387.68	0.106	3
	2	387.58	0.016	3
	3	387.72	0.039	4
7	1	387.7	0.074	3
	2	387.57	0.054	2
	3	387.59	0.028	4
8	1	387.73	0.054	3
	2	387.6	0.015	2
	3	387.58	0.051	4
9	1	387.75	0.067	3
	2*	-	-	-
	3	387.82	0.059	4
10	1	387.71	0.116	3
	2	387.56	0.004	2
	3	387.61	0.061	4
11	1	387.68	0.052	3
	2	387.65	0.017	3
	3	387.47	0.031	4
12	1	387.72	0.081	3
	2	387.57	0.036	2
	3*	-	-	-

Flask analysis results: CH_4

Flask No.	Sampling cycle	$\bar{x}$ (ppb)	s (ppb)	n
1	1	1929.33	1.399	4
	2	1927.74	0.232	2
	3	1932.65	1.524	3
3	1	1931.67	1.074	3
	2	1928.02	0.699	2
	3	1931.59	1.481	5
4	1	1931.62	1.057	3
	2	1929.59	1.963	2
	3	1930.04	0.264	5
5	1	1930.14	0.488	3
	2	1929.07	0.347	2
	3	1930.09	0.011	4
6	1	1930.63	0.709	3
	2	1931.06	2.348	3
	3	1930.8	0.828	4
7	1	1930.65	1.075	3
	2	1929.87	1.962	2
	3	1931.3	1.033	4
8	1	1929.36	2.072	3
	2	1929.62	0.834	2
	3	1928.94	1.573	4
9	1	1932.94	1.943	3
	2*	-	-	-
	3	1927.99	0.527	4
10	1	1931.02	0.581	3
	2	1929.69	1.358	2
	3	1931.1	1.119	4
11	1	1929.48	0.346	3
	2	1928.43	0.952	3
	3	1928.22	1.195	4
12	1	1930.88	1.527	3
	2	1929.44	1.419	2
	3*	-	-	-

Flask analysis results: N_2O

Flask No.	Sampling cycle	$\bar{x}$ (ppb)	s (ppb)	n
1	1	324.42	0.242	3
	2	323.93	0.24	2
	3	323.62	0.208	2
3	1	323.89	0.168	3
	2	324.22	0.093	2
	3	324.44	0.170	3
4	1	324.24	0.225	3
	2	324.03	0.08	3
	3	324.23	0.305	2
5	1	324.39	0.114	3
	2	323.72	0.021	2
	3	324.04	0.412	2
6	1	324.14	0.172	3
	2	324.02	0.086	3
	3	323.9	0.05	2
7	1	324.21	0.23	3
	2	324.25	0.199	2
	3	324.05	0.142	2
8	1	323.99	0.252	3
	2	323.91	0.175	2
	3	323.85	0.098	2
9	1	324.54	0.063	3
	2*	-	-	-
	3	324.2	0.036	2
10	1	323.87	0.18	3
	2	323.95	0.189	2
	3	323.94	0.099	2
11	1	323.51	0.074	3
	2	324.42	0.253	2
	3	323.91	0.099	2
12	1	324.02	0.119	3
	2	324.24	0.247	2
	3*	-	-	-

Flask analysis results: SF_6

Flask No.	Sampling cycle	$\bar{x}$ (ppt)	s (ppt)	n
1	1	20.8	0.024	3
	2	20.78	0.075	2
	3	20.79	0.031	2
3	1	20.85	0.071	3
	2	20.74	0.012	2
	3	20.85	0.149	2
4	1	20.85	0.086	3
	2	20.8	0.081	2
	3	20.83	0.065	2
5	1	20.79	0.089	3
	2	20.72	0.052	2
	3	20.76	0.039	2
6	1	20.82	0.049	3
	2	20.71	0.093	2
	3	20.79	0.027	2
7	1	20.94	0.025	3
	2	20.73	0.007	2
	3	20.78	0.061	2
8	1	20.97	0.09	3
	2	20.7	0.045	2
	3	20.73	0.002	2
9	1	20.92	0.069	3
	2*	-	-	-
	3	20.76	0.024	2
10	1	20.92	0.04	3
	2	20.7	0.0005	2
	3	20.73	0.013	2
11	1	20.9	0.047	3
	2	20.72	0.024	2
	3	20.73	0.046	2
12	1	20.87	0.001	3
	2	20.75	0.063	2
	3*	-	-	-

Flask analysis results: CO

Flask No.	Sampling cycle	$\bar{x}$ (ppb)	s (ppb)	n
1	1	141.19	0.193	3
	2	142.22	0.113	2
	3	142.69	0.607	2
3	1	141.29	0.221	3
	2	142.13	0.158	2
	3	142.88	0.47	2
4	1	141.46	0.064	3
	2	142.05	0.285	2
	3	143.23	0.041	2
5	1	141.69	0.417	3
	2	141.83	0.044	2
	3	143.14	0.039	2
6	1	141.65	0.173	3
	2	142.44	0.081	2
	3	143.06	0.127	2
7	1	142.07	0.043	3
	2	142.13	0.573	2
	3	143.15	0.101	2
8	1	142.01	0.359	3
	2	142.1	0.15	2
	3	143.05	0.246	2
9	1	142.42	0.262	3
	2*	-	-	-
	3	144.47	0.176	2
10	1	142.34	0.047	3
	2	141.87	0.129	2
	3	143.14	0.447	2
11	1	142.49	0.183	3
	2	142.94	0.381	2
	3	143.81	0.1	2
12	1	142.28	0.353	3
	2	141.87	0.215	2
	3*	-	-	-

Flask analysis results: H_2

Flask No.	Sampling cycle	$\bar{x}$ (ppb)	s (ppb)	n
1	1	566.85	0.195	3
	2	564.58	0.637	2
	3	565.55	0.423	2
3	1	566.64	0.088	3
	2	565.2	0.442	2
	3	566.55	1.23	2
4	1	565.48	1.236	3
	2	566.98	1.244	2
	3	567.27	2.989	2
5	1	565.85	0.249	3
	2	564.95	1.205	2
	3	568.73	1.62	2
6	1	566.02	1.786	3
	2	564.62	0.296	2
	3	567.55	2.802	2
7	1	565.03	2.376	3
	2	565.07	0.145	2
	3	568.07	0.252	2
8	1	566.04	1.203	3
	2	564.12	0.771	2
	3	566.21	0.383	2
9	1	564.21	1.615	3
	2*	-	-	-
	3	557.06	1.082	2
10	1	564.55	0.219	3
	2	566.27	0.605	2
	3	565.91	1.052	2
11	1	566.12	2.05	3
	2	564.49	1.127	2
	3	567.59	1.368	2
12	1	566.69	1.254	3
	2	564.48	0.687	2
	3*	-	-	-

Appendix 4: Flask Analysis Results of the Intercomparison Experiment

Note that Mean values are rounded to two significant numbers. Standard deviations are rounded to three significant numbers.

Flask	Sampling time (GMT)	CO_2			CH_4		
		$\bar{x}$ (ppm)	s (ppm)	n	$\bar{x}$ (ppb)	s (ppb)	n
1*	2010-06-07 10:01:22	-	-	-	-	-	-
2*	2010-06-07 10:37:28	-	-	-	-	-	-
3	2010-06-07 11:11:13	382.37	0.06	4	1880.09	1.636	4
4	2010-06-07 11:40:30	375.77	0.078	4	1895.52	1.257	4
5	2010-06-07 12:11:16	379.84	0.057	4	1893.82	1.09	4
6	2010-06-07 12:42:00	377.19	0.061	4	1896.44	1.776	3
7	2010-06-07 13:13:38	382.39	0.093	4	1887.8	1.37	4
8	2010-06-07 13:43:56	382.01	0.046	4	1889.6	0.842	3
9	2010-06-07 14:16:22	380.82	0.044	4	1890.22	1.754	4
10	2010-06-07 14:47:09	380.17	0.085	4	1901.29	1.519	4
11	2010-06-07 15:17:54	382.01	0.065	4	1898.48	0.973	4
12	2010-06-07 15:48:41	381.62	0.077	4	1901.49	1.883	4

*Flasks were subjected to valve breakage.

Appendix 5: Statistics Formulas

$$\bar{x}_W = \frac{\sum(\bar{x}_i \cdot n_i)}{\sum n_i}$$

$$s_W = \sqrt{\frac{\sum s_i^2 \cdot (n_i - 1)}{\sum n_i - k}}$$

$$s_{w[x_1 - x_2]} = \sqrt{s^2_{w[x_1]} + s^2_{w[x_2]}}$$

$$SE_{w[x_1 - x_2]} = \frac{s_{w[x_1 - x_2]}}{\sqrt{n_1 + n_2}}$$

where: $\bar{x}_W$ = weighted mean

$\bar{x}_i$ = arithmetic mean

n_i = repetition of measurements

s_W = weighted standard deviation

s_i = sample standard deviation

k = number of sampling cycles

$s_{w[x_1 - x_2]}$ = weighted standard deviation for two stochastic variables

$SE_{w[x_1 - x_2]}$ = weighted standard error for two stochastic variables

References

1. Conway TJ, Tans PP, Waterman LS, Thoning KW. Evidence for interannual variability of the carbon cycle from the National Oceanic and Atmospheric Administration Climate Monitoring and Diagnostics Laboratory Global Air Sampling Network. J Geophys Res. 1994 Nov 20;99(D11):22831-55.
2. Conway TJ, Tans PP. Atmospheric carbon dioxde mixing ratios from the NOAA Climate Monitoring and Diagnostics Laboratory Cooperative Flask Sampling Network, 1967-1993. CDIAC/NDP-005R3, Carbon Dioxide Information Center, Oak Ridge National Laboratory, Oak Ridge, Tennessee, USA, 1996.
3. Conway TJ, Tans P, Waterman LS, Thoning KW, Masarie K, Gammon R. Atmospheric carbon dioxide measurements in the remote global troposphere, 1981–1984. Tellus B Chem Phys Meteorol. 1987;408(2):81-115.
4. Machida T, Matsueda H, Sawa Y, Nakagawa Y, Hirotani K, Kondo N, et al. Worldwide measurements of atmospheric CO2 and other trace gas species using commercial airlines. J Atmos Oceanic Technol. 2008 Oct;25(10):1744-54.
5. Komhyr WD, Gammon RH, Harris TB, Waterman LS, Conway TJ, Taylor WR, et al. Global atmospheric CO2 distribution and variations from 1968-1982 NOAA/GMCC CO2 flask sample data. J Geophys Res. 1985;90:5567-96.
6. Langenfelds RL, Steele LP, Murray DL, Krummel PB, Spencer DA, Fraser PJ. Atmospheric methane, carbon dioxide, carbon monoxide, hydrogen and nitrous oxide from Cape Grim flask air samples analysed by gas chromatography. Melbourne: Bureau of Meteorology and CSIRO Division of Atmospheric Research and CSIRO Marine and Atmospheric Research. 2006.

7. Trolier M, White JWC, Tans PP, Masarie KA, Gemery PA. Monitoring the isotopic composition of atmospheric CO2: Measurements from the NOAA Global Air Sampling Network. J Geophys Res. 1996 Nov 20;101(D20): 25897-916.

8. Keeling CD. The concentration and isotopic abundances of carbon dioxide in the atmosphere. Tellus. 1960;12(2):200-3.

9. Manning AC, Keeling RF. Global oceanic and land biotic carbon sinks from the Scripps atmospheric oxygen flask sampling network. Tellus B Chem Phys Meteorol. 2006 Apr;58(2):95-116.

10. Lodge JP, Intersociety Committee. Methods of air sampling and analysis. 3rd ed. New York; Chelsea: Intersociety Committee. Lewis Publishers; 1989.

11. Gamnitzer U, Karstens U, Kromer B, Neubert REM, Meijer HAJ, Schroeder H, et al. Carbon monoxide: A quantitative tracer for fossil fuel CO2? J Geophys Res. 2006 Nov 18;111:D22302.

12. Theis DE, Saurer M, Blum H, Frossard E, Siegwolf RTW. A portable automated system for trace gas sampling in the field and stable isotope analysis in the laboratory. Rapid Commun Mass Spectrom. 2004;18(18):2106-12.

13. Schauer AJ, Lai CT, Bowling DR, Ehleringer JR. An automated sampler for collection of atmospheric trace gas samples for stable isotope analyses. AGR Forest Meteorol. 2003 Aug 30;118(1-2):113-24.

14. Bakwin PS, Tans PP, Hurst DF, Zhao CL. Measurements of carbon dioxide on very tall towers: results of the NOAA/CMDL program. Tellus B Chem Phys Meteorol. 1998 Nov;50(5):401-15.

15. Neubert REM, Spijkervet LL, Schut JK, Been HA, Meijer HAJ. A computer-controlled continuous air drying and flask sampling system. J Atmos Oceanic Technol. 2004 Apr;21(4):651-9.

16. Forster P, Ramaswamy P, Artaxo P, Berntsen T, Betts R, Fahey DW, et al. Changes in atmospheric constituents and in radiative forcing. In: Solomon S, Qin D, Manning M, Chen Z, Marquis M, Averty K, Tignor MMB & Miller HL (Eds.) Climate Change 2007: The Physical Science Basis. Contribution of Working Group I to the Fourth Assessment Report of the Intergovernmental Panel on Climate Change. Cambridge; 2007.
17. University of Colorado at Boulder. Monitoring of carbon dioxide will require global data collection ten times larger than current set up. 2008 Apr 29 [cited 2010 May 20]. ScienceDaily. Available from: http://www.sciencedaily.com/releases/2008/04/080424141929.htm.
18. ICOS Satkeholder's Handbook 2008
19. ICOS Stakeholder's Handbook 2009
20. European Commission. The ICOS project: balancing Europe's carbon budget. 2008 Dec 12 [cited 2010 Jan 12]. Available from: http://cordis.europa.eu/fetch?CALLER=FP7_NEWS&ACTION=D&RCN=30242.
21. Hofmann DJ, Butler JH, Dlugokencky EJ, Elkins JW, Masarie K, Montzka SA, et al. The role of carbon dioxide in climate forcing from 1979 to 2004: introduction of the Annual Greenhouse Gas Index. Tellus B Chem Phys Meteorol. 2006 Nov;58(5):614-9.
22. Boden TA, Marland G, Andres RJ. Global, regional, and natinal fossil-fuel CO2 Emissions. Carbon Dioxide Information Analysis Center, Oak Ridge National Laboratory, U.S. Department of Energy, Oak Ridge, Tennessee, USA; 2009.
23. Le Quere C, Raupach MR, Canadell JG, Marland G, Bopp L, Ciais P, et al. Trends in the sources and sinks of carbon dioxide. Nat Geosci. 2009 Dec; 2(12):831-6.

24. Houghton RA. Carbon flux to the atmosphere from land-use-change: 1850-2005. Carbon Dioxide Information Analysis Center, Oak Ridge National Laboratory, U.S. Department of Energy, Oak Ridge, Tennessee, USA; 2008.

25. Nakicenovic N, Alcamo J, Davis G, de Vries B, Fenhann J, Graffin S. Special Report on Emission Scenarios: Intergovernmental Panel on Climate Change; 2000.

26. Wuebbles DJ, Hayhoe K. Atmospheric methane and global change. Earth-Sci Rev. 2002 May;57(3-4):177-210.

27. Graedel TE, Crutzen PJ. Atmospheric change : an Earth system perspective. New York: W.H. Freeman; 1993.

28. Dlugokencky EJ, Houweling S, Bruhwiler L, Masarie KA, Lang PM, Miller JB, et al. Atmospheric methane levels off: Temporary pause or a new steady-state? Geophys Res Lett. 2003 Oct 8;30(19).

29. Dlugokencky EJ, Bruhwiler L, White JWC, Emmons LK, Novelli PC, Montzka SA, et al. Observational constraints on recent increases in the atmospheric CH4 burden. Geophys Res Lett. 2009 Sep 17;36(L18803).

30. Flückiger J, Dallenbach A, Blunier T, Stauffer B, Stocker TF, Raynaud D, et al. Variations in atmospheric N2O concentration during abrupt climatic changes. Science. 1999 Jul 9;285(5425):227-30.

31. Kroeze C, Mosier A. New estimates for emissions of nitrous oxide. Non-CO2 greenhouse gases: Scientific understanding, control and implementation. 2000:45-64.

32. Warneck P. Chemistry of the natural atmosphere. 2nd ed. San Diego: Academic Press; 2000.

33. Ravishankara AR, Daniel JS, Portmann RW. Nitrous Oxide (N2O): The dominant ozone-depleting substance emitted in the 21st Century. Science. 2009 Oct 2;326(5949):123-5.

34. Busenberg E, Plummer LN. Dating groundwater with trifluoromethyl sulfurpentafluoride (SF5CF3), sulfur hexafluoride (SF6), CF3Cl (CFC-13), and CF2Cl2 (CFC-12). Water Resour Res. 2008 Feb 22;44(2):3011-30.

35. Maiss M, Brenninkmeijer CAM. Atmospheric SF6: Trends, sources, and prospects. Environ Sci Technol. 1998 Oct 15;32(20):3077-86.

36. Maiss M, Brenninkmeijer CAM. A reversed trend in emissions of SF6 into the atmosphere? Non-CO2 greenhouse gases: Scientific understanding, control and implementation. 2000:199-204.

37. Khalil MAK, Rasmussen RA. The global cycle of carbon monoxide: Trends and mass balance. Chemosphere. 1990;20(1-2):227-42.

38. Novelli PC, Masarie KA, Lang PM. Distributions and recent changes of carbon monoxide in the lower troposphere. J Geophys Res. 1998 Aug 20;103(D15): 19015-33.

39. Novelli PC, Lang PM, Masarie KA, Hurst DF, Myers R, Elkins JW. Molecular hydrogen in the troposphere: Global distribution and budget. J Geophys Res. 1999 Dec 20;104(D23):30427-44.

40. Khalil MAK, Rasmussen RA. Global increase of atmospheric molecular hydrogen. Nature. 1990 Oct 25;347(6295):743-5.

41. Keeling RF. Measuring correlations between atmospheric oxygen and carbon dioxide mole fractions - a preliminary-study in urban air. J Atmos Chem. 1988 Aug;7(2):153-76.

42. Keeling RF, Najjar RP, Bender ML, Tans PP. What atmospheric oxygen measurements can tell us about the global carbon cycle. Global Biogeochem Cycles. 1993 Mar;7(1):37-67.

43. Keeling RF, Shertz SR. Seasonal and interannual variations in atmospheric oxygen and implications for the global carbon cycle. Nature. 1992 Aug 27;358(6389):723-7.

44. Machta L, Hughes E. Atmospheric oxygen in 1967 to 1970. Science. 1970;168(3939):1582-4.

45. Fry B. Stable isotope ecology. New York, NY: Springer; 2006.

46. Mook WG. Introduction: Theory, methods, review. Paris: United Nations Educational, Scientific and Cultural Organization & International Atomic Energy Agency; 2000.

47. Yakir D, Sternberg LDL. The use of stable isotopes to study ecosystem gas exchange. Oecologia. 2000 May;123(3):297-311.

48. Gemery PA, Trolier M, White JWC. Oxygen isotope exchange between carbon dioxide and water following atmospheric sampling using glass flasks. J Geophys Res. 1996 Jun 20;101(D9):14415-20.

49. Levin I, Hesshaimer V. Radiocarbon - A unique tracer of global carbon cycle dynamics. Radiocarbon. 2000;42(1):69-80.

50. Suess HE. Radiocarbon Concentration in Modern Wood. Science. 1955;122(3166):415-7.

51. Levin I, Hammer S, Kromer B, Meinhardt F. Radiocarbon observations in atmospheric CO2: Determining fossil fuel CO2 over Europe using Jungfraujoch observations as background. Sci Total Environ. 2008 Mar 1;391(2-3):211-6.

52. Tans PP, Bakwin PS, Guenther DW. A feasible global carbon cycle observing system: A plan to decipher today's carbon cycle based on observations. Glob Chang Biol. 1996 Jun;2(3):309-18.

53. Andrews AE, Bruhwiler L, Crotwell AM, Dlugokencky EJ, Hahn MP, Hirsch AI, et al. Carbon Cycle Greenhouse Gases. Boulder: National Oceanic and Atmospheric Administration; 2003.

54. Sturm P, Leuenberger M, Sirignano C, Neubert REM, Meijer HAJ, Langenfelds R, et al. Permeation of atmospheric gases through polymer O-rings used in flasks for air sampling. Journal of Geophysical Research-Atmospheres. 2004 Feb 25;109(D4).

55. Peacock RN. Practical selection of elastomer materials for vacuum seals. J Vac Sci Technol. 1980;17(1):330-6.

56. Parker Hannifin Corporation. Parker O-ring handbook; 2001.

57. Ma C, Shero E, Verma N, Gilbert SL, Shadman F. Permeation of moisture and oxygen through polymeric O-rings. Ies J. 1995 Mar-Apr;38(2):43-6.

58. Rothe M, Jordan A, Brand WA. Trace Gases, δ13C and δ18O of CO2-in-air samples: Storage in glass flasks using PCTFE seals and other effects. In: Worthy D, Huang L, editors. 12th WMO/IAEA Meeting of Experts on Carbon Dioxide Concentration and Related Tracers Measurement Techniques; Toronto: World Meteorological Organization; 2003.

59. Brand WA, editor. O2/N2 storage aspects and open split mass spectrometric determination. In: Worthy D, Huang L, editors. 12th WMO/IAEA Meeting of Experts on Carbon Dioxide Concentration and Related Tracers Measurement Techniques; 2003; Toronto: World Meteorological Organization; 2005.

60. Mann CA. Leak Testing. Non-Destructive Testing. 1968;1(5):237-41.

61. Glück B. Hydrodynamische und gasdynamische Rohrströmungen; Druckverluste. Berlin: VEB Verlag für Bauwesen; 1988.

62. Durst F. Fluid mechanics : an introduction to the theory of fluid flows. Berlin: Springer; 2008.

63. Keeling RF, Manning AC, Paplawsky WJ, Cox AC. On the long-term stability of reference gases for atmospheric O-2/N-2 and CO2 measurements. Tellus B Chem Phys Meteorol. 2007 Feb;59(1):3-14.

64. Jordan A, Brand WA, editors. Technical Report: MPI-BGC, Germany. Report of the 11th WMO/IAEA Meeting of Experts on Carbon Dioxide Concentration and Related Tracers Measurement Techniques; 2001; Tokyo: World Meteorological Organization.

65. Sachs L, Hedderich J. Angewandte Statistik: Methodensammlung in R. Berlin; Heidelberg; New York: Springer; 2006.

66. Zhang C. Fundamentals of environmental sampling and analysis. Hoboken, N.J.: Wiley-Interscience; 2007.

67. Uglietti C, Leuenberger M, Valentino FL. Comparison between real time and flask measurements of atmospheric O2 and CO2 performed at the High Altitude Research Station Jungfraujoch, Switzerland. Sci Total Environ. 2008 Mar 1;391(2-3):196-202.

68. Winderlich J, Chen H, Höfer A, Gerbig C, Seifert T, Kolle O, et al. Continuous low-maintenance CO2/CH4/H2O measurements at the Zotino Tall Tower Observatory (ZOTTO) in Central Siberia. Atmos Meas Tech Discuss.3(2): 1399-437.

69. Thompson RL, Manning AC, Gloor E, Schultz U, Seifert T, Hänsel F, et al. In-situ measurements of oxygen, carbon monoxide and greenhouse gases from Ochsenkopf tall tower in Germany. Atmos Meas Tech. 2009;2(2):573-91.

70. Popa ME. Continuous tall tower multispecies measurements in Europe for quantifying and understanding land-atmosphere carbon exchange. Jena: Friedrich-Schiller-Universität Jena; 2007.

71. Rella C. Accurate greenhouse gas measurements in humid gas streams using the Picarro G3101 carbon dioxide / methane / water vapor gas analyzer. White Paper. 2009.

72. Chen H, Winderlich J, Gerbig C, Hoefer A, Rella CW, Crosson ER, et al. High continuous airborne measurements of greenhouse gases (CO2 and CH4) using the cavity ring-down spectroscopy (CRDS) technique. Atmos Meas Tech. 2010;3:375-86.

73. Abramczyk H. Introduction to laser spectroscopy. 1st ed. Amsterdam; Boston: Elsevier; 2005.

74. Picarro. WS-CRDS - A universal instrument for precise measurement of GHGs. White Paper. 2008.

75. Ball SM, Jones RL. Broad-band cavity ring-down spectroscopy. Chem Rev. 2003 Dec;103(12):5239-62.

76. Crosson ER. A cavity ring-down analyzer for measuring atmospheric levels of methane, carbon dioxide, and water vapor. Appl Phys B. 2008 Sep;92(3): 403-8.

List of Figures

List of Tables

Acknowledgements

First of all, I would like to thank my supervisor from the MPI-BGC, Dr. Christoph Gerbig, who gave me the unique opportunity to write my diploma thesis in a frame of such an important and ambitious research project like ICOS, and I always felt it as a great privilege to make my contribution to it. I want to thank him for his continuous support, encouragement and patience. His experience about experimental design and his ability to explain things in a very precise way have always been of great help. I am also grateful to him for having been able to take part at the 8th International Carbon Dioxide Conference and at several field campaigns for aircraft sampling to get a deeper look into the everyday life of a scientist in global carbon cycle research.

I am grateful to Prof. Dr. Bernd Rudolph from the University of Applied Science Jena who spontaneously agreed to supervise me, and for all of his efforts and patience during my study as a professor from my environmental chemistry and instrumental methods of analysis courses.

Special thanks goes to Dave Senders from High Precision Devices Inc. for his comprehensive support throughout the evaluation process and his willingness to share important documents with me.

I would also like to show my gratitude to Dr. Jošt V. Lavriče who was my first contact from the ICOS coordination staff at Paris. Later he moved to Jena to start as a group leader for the MPI-BGC Tall Tower Network. Here in Jena he had not to care about me and "my sampler" any longer but he was still interested in my work and I thank him for that as well as for helpful discussions about the ICOS project.

My sincere thanks goes to my office mate Michael Hielscher for preparing the reference air mixtures and for taking all the photos.

In particular, I would like to thank Karl Kübler and Reimo Leppert for their technical support on the dryer. Their practical knowledge and expertise have frequently helped me out of several problems. I am grateful for their time and their kind willingness to help. I also thank Bernd Schlöffel and Frank Voigt from the MPI-BGC Mechanical Workshop for customizing the pistons and for many interesting information about machine-tool operations. In addition to the workshop team, I like to thank Dr. Armin Jordan and Bert Steinberg from the MPI-BGC GasLab for their effort in analysis of the flask samples.

I am most grateful to Stefanie Riedel and Jonas Schneider for proofreading my diploma thesis. Stefanie always encouraged me to use the gerund more often and Jonas provided me with important suggestions which helped me not to break elementary rules of scientific writing. Both are not familiar with atmospheric air sampling technologies but their efforts have helped significantly in turning my original diploma thesis into a readable and useful document.

I would also like to show my gratitude to Julia Steinbach for many scientific discussions about flask sampling and how to create elegant plots with R; Roberto Kretschmer for several useful tips in R-programming; Jan Winderlich and Huilin Chen for their help with the CRDS analyzer and their interest in my work; and Thomas Seifert, who offered me a warm welcome at the institute when I started there as a students helper as well as for his enthusiasm in motivating me.

I like to thank my friends in Jena Hendrik Zöphel, Sebastian Gimper and Sebastian Klein for their constant friendship and encouragement.

Finally, I have to thank my mother for her love and support during my entire education. Thank you mom!

Erklärung

Ich erkläre, daß ich die vorliegende Diplomarbeit selbständig und nur unter Verwendung der angegebenen Quellen und Hilfsmittel angefertigt habe.

Jena, den 29.06.2010

_____

Stephan Baum